WATER RESOURCES RESEARCH, VOL. 49, 4952–4970, doi:10.1002/wrcr.20380, 2013

Geochemical and geophysical responses during the infiltration of fresh water into the contaminated saprolite of the Oak Ridge Integrated Field Research Challenge site, Tennessee

A. Revil,[1,2] Y. Wu,[3] M. Karaoulis,[2] S. S. Hubbard,[3] D. B. Watson,[4] and J. D. Eppehimer[1]

Received 10 December 2012; revised 17 June 2013; accepted 19 June 2013; published 12 August 2013.

[1] At the Oak Ridge Integrated Field Research Challenge (IFRC) site, Tennessee, the saprolitic aquifer was contaminated by leaks from the former S-3 disposal ponds between 1951 and 1983. The chemistry of the contaminant plume is also episodically impacted by fresh meteoritic water infiltrating vertically from a shallow variably saturated perched zone and the ditch surrounding the former S-3 ponds. We performed a column experiment using saprolite from the contaminated aquifer to understand the geochemical and complex electrical conductivity signatures associated with such events. The changes in the pH and pore water ionic strength are responsible for measurable changes in both the in-phase and quadrature conductivities. The pore water conductivity can be related to the nitrate concentration (the main ionic species in the plume) while the release of uranium is controlled by the pH. We developed a simple model to determine the pore water conductivity and pH from the recorded complex conductivity. This model is applied to time-lapse resistivity data at the IFRC site. Time-lapse inversion of resistivity data, performed with an active time constrain approach, shows the occurrence of an infiltration event during the winter of 2008–2009 with a dilution of the pore water chemistry and an increase of the pH. A simple numerical simulation of the infiltration of fresh water into the unconfined contaminated aquifer is consistent with this scenario.

Citation: Revil, A., Y. Wu, M. Karaoulis, S. S. Hubbard, D. B. Watson, and J. D. Eppehimer (2013), Geochemical and geophysical responses during the infiltration of fresh water into the contaminated saprolite of the Oak Ridge Integrated Field Research Challenge site, Tennessee, *Water Resour. Res.*, *49*, 4952–4970, doi:10.1002/wrcr.20380.

1. Introduction

[2] The Oak Ridge Integrated Field Research Challenge (OR-IFRC) site is a Department of Energy (DOE) test site located near Oak Ridge, Tennessee. This site was established to understand the migration of various contaminants from the former S-3 disposal ponds (located in the Bear Creek Valley, Figure 1) into the surrounding saprolitic aquifer [*Watson et al.*, 2004]. The S-3 disposal ponds consisted of four ponds built in 1951. They received a yearly volume of 7.6 million liters of acidic (pH < 2) liquid wastes consisting of nitric acid, uranium, technetium, cadmium, mercury, and chlorinated solvents for 32 years [*Shevenell et al.*, 1994]. The wastes were disposed of in liquid acid form so the contaminants could readily migrate away from the ponds and precipitate when encountering carbonate-rich high pH-buffered zones. As a result, there is a reservoir of contaminants in the saprolite and rock matrix beneath the ponds. In 1983, the ponds were drained and filled with fill materials to neutralize the acidic waste waters. The four disposal ponds were covered with a multilayer cap (including an asphalt cap) resulting in minimal leaching from the surface. The meteoric water falling on this cap is presently diverted in a ditch surrounding the former S3 basins. The primary mechanism of contaminant transport is therefore groundwater flow through the underlying contaminated materials.

[3] Understanding contaminant transport from the former S-3 Ponds is a key component of the remediation program undertaken at Oak Ridge. One of the difficulties is that the properties of the saprolite are not well understood. The saprolite is the result of shale and limestone weathering and is rich in illite and smectite. The clay content and mineralogy play an important role in controlling the specific surface area of clay-rich materials and therefore their petrophysical properties including permeability and porosity [*Revil and Cathles*, 1999; *McKay et al.*, 2000; *Watson et al.*, 2004].

[4] The relatively high amounts of clay minerals also play a role, as discussed below, on the electrical resistivity. Electrical resistivity tomography could be used in turn to

[1]Department of Geophysics, Colorado School of Mines, Golden, Colorado, USA.
[2]ISTerre, CNRS, UMR CNRS 5275, Université de Savoie, Le Bourget du Lac, France.
[3]Lawrence Berkeley National Laboratory, Berkeley, California, USA.
[4]Oak Ridge National Laboratory, Oak Ridge, Tennessee, USA.

Corresponding author: A. Revil, Department of Geophysics, Colorado School of Mines, Golden, CO 80401, USA. (arevil@mines.edu)

©2013. American Geophysical Union. All Rights Reserved.
0043-1397/13/10.1002/wrcr.20380

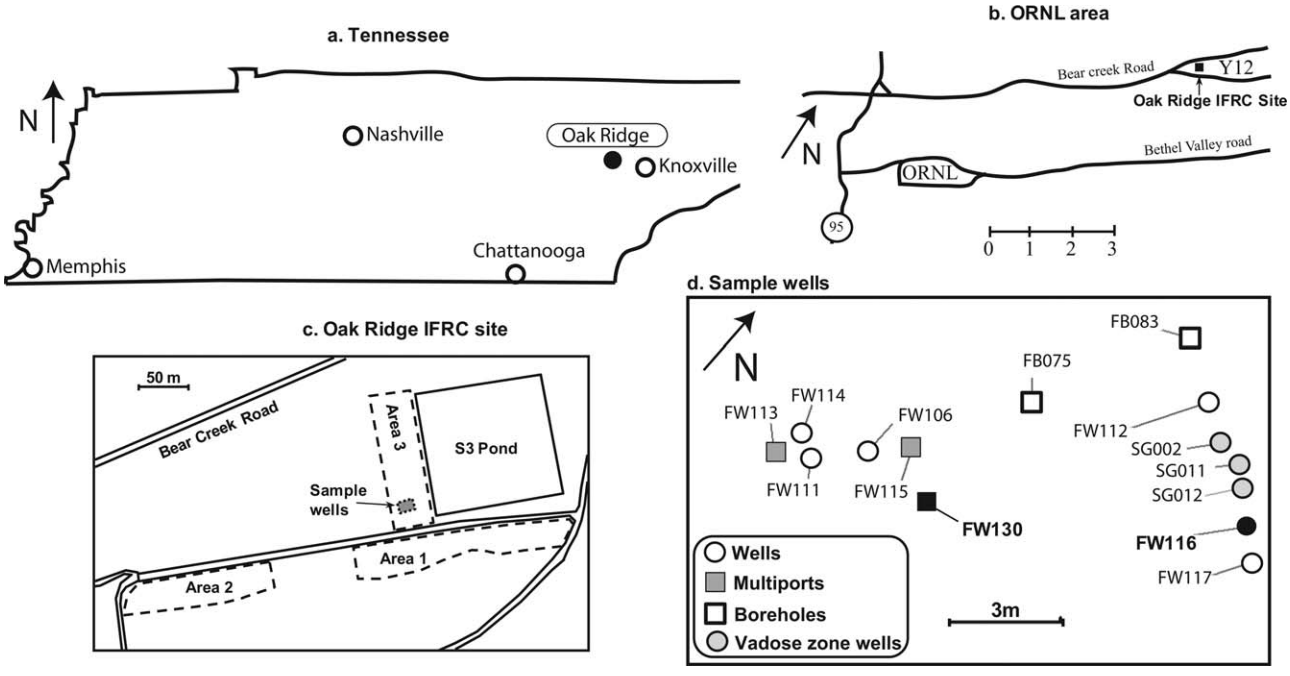

Figure 1. Position of the wells where the ground water was sampled. (a) Location of Oak Ridge in Tennessee. (b) Position of the Oak Ridge IFRC test site. (c) Position of area 3 downstream the former S-3 disposal ponds. (d) Position of the wells FW130 used to sample the contaminated ground water sampled at a depth of ~15 m and Well FW116 used to sample the fresh ground water from the shallow portion of the aquifer at a depth of ~2 m. SG012 is in the very shallow perched zone.

locate the position of the contaminant plumes and monitor the changes in the concentration of the contaminants. Indeed, a number of recent geophysical studies [*Kowalsky et al*., 2011; *Gasperikova et al*., 2012; *Revil et al*., 2013a] have focused on determining the extent of the plumes associated with contaminant migration from the former S-3 disposal ponds as well as evaluating the potential for natural attenuation of these plumes. Recently, *Revil et al*. [2013a, 2013b, 2013c] have pointed out that the interpretation of resistivity data cannot be properly done without taking into account the surface conductivity associated with the presence of clay minerals. That said, the *Revil et al*. [2013a] study was conducted with samples from the uncontaminated background site keeping only the fine fraction of the saprolite and using a simple NaCl solution as the leachate to conduct the experiments. No electrical conductivity experiments have been performed to date on contaminated saprolites (which have experienced acidic solution for a long time) and with the natural pore waters found at the site. Such investigations are however required to understand the interfacial (surface) electrical conductivity and quadrature conductivity and their relationship to the presence of the contaminants.

[5] The main point of our study is to address how the geochemistry of the contaminant plume is influenced by infiltration events of fresh (meteoritic) water. The interaction between the fresh, oxic, neutral water from the perched zone and the contaminated water influences the geochemistry of the contaminated saprolite saturated by acidic, reduced, pore water. These infiltration events are associated with the episodic recharges to the regional water table associated with rainfall infiltration. There is therefore a need to quantify spatially these geochemical changes using time-lapse geophysical monitoring in order to assess natural attenuation mechanisms and to select effective remediation techniques.

[6] Spectral-induced polarization (SIP, complex conductivity) is a nonintrusive geophysical method that can be used to image contaminant plumes (*Flores Orozco et al*. [2012]), to determine permeability [*Revil and Florsch*, 2010], and to monitor interfacial electrochemistry at the pore water mineral interface [*Vaudelet et al*., 2011a, 2011b]. Induced polarization has a long history of use in colloidal chemistry and geophysics, and various petrophysical models have been developed over time to determine the relationship between the in-phase and quadrature conductivities and the texture of the material as well as the electrochemical properties of the mineral water interface [*de Lima and Sharma*, 1992; *Grosse*, 2011]. Recent work has focused on the development of a new model based on the polarization of the Stern layer to describe spectral induced polarization of clayey materials with simple supporting electrolytes (e.g., NaCl or KCl) [*Revil and Florsch*, 2010; *Weller et al*., 2011; *Revil*, 2012, 2013; *Revil et al*., 2013a, 2013c].

[7] In the present study, we investigate how spectral induced polarization can be used in the laboratory to monitor changes in the pore water and interfacial chemistry in a complex porous material (the contaminated saprolite mentioned above) and with natural ground water from the less-contaminated shallow aquifer and underlying plume of highly contaminated groundwater. To establish the relationship between induced polarization and geochemistry needed to interpret field data, we performed a column

experiment to simulate the type of infiltration occurring in the field. Both the saprolite core and the ground waters were sampled from the OR-IFRC research site. These results are then used to interpret time-lapse resistivity data to monitor one of the main contaminant plumes (the CP1 plume) during an infiltration event and to interpret these results in terms of change in the pore water chemistry.

2. Background

[8] The location of the OR-IFRC research site is shown in Figures 1a and 1b. The position of the former S-3 disposal ponds and the two wells used in our study (the shallow well FW116 and the deeper well FW130) are shown in Figures 1c and 1d, respectively. The contaminant plumes results from the release of the contaminants stored in the clayey matrix below the former S-3 ponds in the saprolitic aquifer. The perched aquifer sketched in Figure 2 results mostly from transient infiltration of meteoritic waters from the ditch surrounding the former S-3 ponds. Well FW116 (about 6 m deep) is screened at the very top of the water table where water from the perched zone has percolated down and is therefore less contaminated than at greater depths. It samples the upper portion of the saprolitic aquifer.

[9] The main scientific question we address is how the contaminants contained in the saprolitic aquifer are episodically affected by fresh water infiltration from the perched aquifer (see Figure 2) and if this mixing can be monitored by time-lapse electrical methods (resistivity and induced polarization imaging). Change in the pore chemistry includes dilution and pH changes, which in turn trigger sorption and desorption mechanism on the surface of the clays.

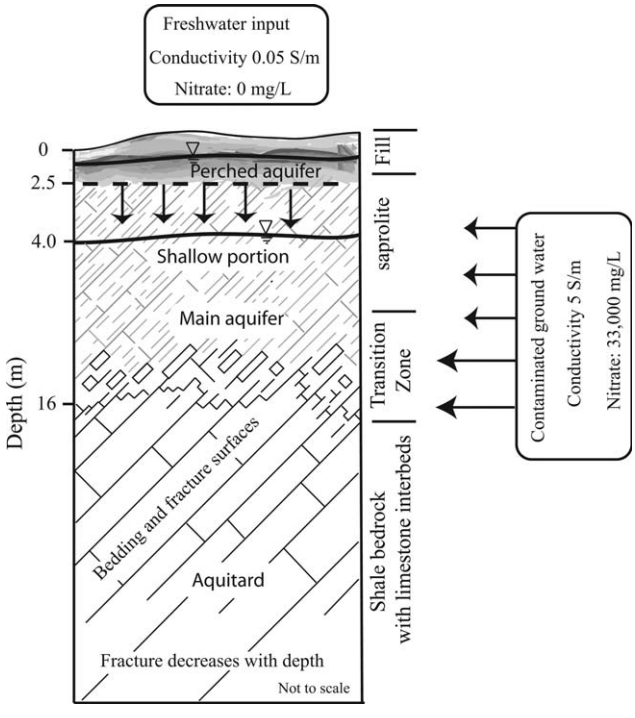

Figure 2. Position of the problem. Typical section of saprolite and parent rock at the Oak Ridge Integrated Field Research Challenge (IFRC) site. The transition zone at the bottom of the saprolitic aquifer is an area of higher permeability than the upper portion of the aquifer. Water infiltration can come either from the perched aquifer or from a ditch located in the vicinity of the S-3 pond. The shallow portion of the aquifer (sampled by the shallow Well F116) is influenced by the pervasive infiltration from the shallow aquifer.

[10] The saprolite material used in the column experiment described in section 4 was cored from Well FW130 (Figure 1d) at a depth of ~15 m. This sample is therefore from the transition zone between the saprolite and the basement rock. This zone is usually considered to have an enhanced permeability with respect to the upper more clay-rich portion of the saprolite and is locally very contaminated [*Watson et al.*, 2004]. As explained in section 4, the two types of groundwater were collected from Well FW130 (heavily contaminated ground water sampled at a depth of ~15 m) and Well FW116 (fresh ground water from the less-contaminated upper portion of the saprolitic aquifer). The compositions of the two ground waters are reported in Table 1. All the parameters that we will introduce in our equations are defined in Table 2.

[11] During the mixing of the freshwater and the contaminated ground water, two key parameters that should be monitored are the conductivity of the pore water and the pH. The conductivity of the water can be related to the nitrate concentration by (Figure 3):

$$\sigma_w(25^\circ\mathrm{C}, C_N) = \sigma_w(25^\circ\mathrm{C}, \mathrm{Background}) + 1.4 \times 10^{-4} C_N(\mathrm{mg/L}). \quad (1)$$

[12] The data shown in Figure 3 means that the concentration in nitrate are a good proxy for estimating the conductivity of the pore water in isothermal conditions. These data do not imply necessarily that other ions have negligible effects on the pore water conductivity. To be consistent with the data reported in Table 1 for the upper portion of the aquifer, the background conductivity of the pore water is taken equal to 0.03 S m^{-1} at 25°C for the perched water. Indeed, the nitrate concentration in the perched aquifer is

Table 1. Composition of the Ground Water Samples Used for the Experiment[a]

Parameter	FW116	FW130
pH	6.54	3.8
Fluid conductivity (S m^{-1})	0.067	2.08
Dissolved O_2	0.6	0.19
Ca	50.8	1429
Mg	5.8	231.5
Na	272.7	752
K	9.4	1133
SO_4	31.2	196.6
NO_3	254.5	14,335
Al	110.4	533.8
Mn	1.32	231.6
Fe	BDL	26.3
U	0.47	14.8
Sr	0.65	3

[a]Ground water sample F116 denotes the relatively fresh water in the upper (nearly uncontamined) portion of the aquifer. Sample FW130 refers to the deeper contaminated ground water. All units in milligram per liter unless specified. BDL: Below detection limit.

Table 2. Definition of the Parameters

Parameter	Unit	Meaning
C_N	Mg L^{-1}	Nitrate concentration
CEC	C kg^{-1}	Cation exchange capacity
C_i^0	Mol L^{-1}	Initial concentration of species i
C_i^∞	Mol L^{-1}	Final concentration of species i
C_i	Mol L^{-1}	Concentration of species i
$\overline{D}$	m^2 s^{-1}	Apparent dispersion coefficient
D	m^2 s^{-1}	Diffusion coefficient
Du*		Complex-valued Dukhin number
Du		Dukhin number (ratio of surface to pore water conductivity)
F		Formation factor
f		Fraction of counterions in the Stern layer ($0 \leq f \leq 1$)
[H$^+$]	M	Proton concentration
i		Pure imaginary number
K_{Na}	L Mol^{-1}	Apparent sorption constant of Na$^+$ in the Stern layer
L	m	Length of the column
M		Cementation exponent
P_L		Peclet number
S_{sp}	m^2 g^{-1}	Specific surface area
[U]	Mol L^{-1}	Uranium concentration
Q_V	C m^{-3}	Excess of charge per unit pore volume
R_d		Retardation factor
T		Number of pore volumes of flow
t	s	Time
$\beta_{(+)}$	m^2 s^{-1}V^{-1}	Mobility of the ions in the pore water
$\beta^S_{(+)}$	m^2 s^{-1}V^{-1}	Mobility of the counterions in the Stern layer
σ_w	mg L^{-1}	Conductivity of the pore water
σ^*	S m^{-1}	Complex conductivity of the porous material
$\lvert\sigma\rvert$	S m^{-1}	Magnitude of the conductivity of the porous material
σ'	S m^{-1}	In-phase (real) conductivity of the porous material
σ''	S m^{-1}	Quadrature (imaginary) conductivity of the porous material
σ_S*	S m^{-1}	Complex surface conductivity
σ''_M	S m^{-1}	High-salinity asymptotic value of the quadrature conductivity
σ_w^0	S m^{-1}	Initial value of the pore water conductivity
σ_w^∞	S m^{-1}	Final value of the pore water conductivity
φ	rad	Phase lag of the complex conductivity
ϕ		Connected porosity
ρ_g	kg m^{-3}	Mass density of the grains
α	m	Longitudinal dispersivity

$C_N \approx 254.5$ mg L^{-1} (Table 1) and therefore equation (1) predicts that the conductivity of the upper portion of the aquifer is 0.07 S m^{-1} at 25°C in excellent agreement with the measured value reported in Table 1 (0.067 S m^{-1}). Equation (1) can also be used to predict the conductivity of the contaminated groundwater in Well FW130 ($C_N \approx 14{,}000$ mg L^{-1}). We obtain 2.07 S m^{-1} at 25°C. This is consistent with the measured value of 2.08 S m^{-1} at 25°C.

[13] The other critical parameter to monitor is the pH of the pore water solution. Indeed, the change in pH can be related to the change in uranium concentration (see Figure 4) according to the following empirical relationship,

$$[\mathrm{U}](\mathrm{mg/L}) = [\mathrm{U}](\mathrm{Background}, \mathrm{mg/L}) + a\{[\mathrm{H}^+] - 10^{-6.4}\}, \tag{2}$$

where [U](mg/L) represents the uranium concentration in mg L^{-1}, [U](Background) denotes the background concentration in uranium in the perched aquifer (at pH 6.4), and [H$^+$] denotes the concentration of protons in Mol L^{-1}. The concentration in uranium is both controlled by the dilution and a source term depending on the pH, which controls the release of uranium from the mineral surface [*Watson et al.*, 2004]. The key of our analysis is therefore to connect the complex conductivity to these two parameters. For this, we decided to perform a column experiment simulating an infiltration experiment in conditions similar to the field.

3. Properties of Saprolitic Core Samples

[14] We first summarize here the experimental results obtained recently in the laboratory by *Revil et al.* [2013b] on core samples from the background (uncontaminated) site at Oak Ridge using a simple supporting electrolyte (NaCl). The goal of this section is to familiarize the reader with the state of knowledge we have on the complex conductivity of saprolites for which, so far, only the fine fraction of the material has been studied.

3.1. Theory

[15] The complex conductivity σ^* of a porous material is written as,

$$\sigma^* = |\sigma|\exp(i\varphi) = \sigma' + i\sigma'', \tag{3}$$

where $|\sigma|$ denotes the amplitude of the conductivity (in S m^{-1}), φ the phase lag (in rad), σ' (≥ 0) and σ'' (≤ 0) denote the real (in phase) and imaginary (quadrature) components of the conductivity (in S m^{-1}), and i denotes the pure imaginary number ($|\sigma| = \sqrt{\sigma'^2 + \sigma''^2}$ and $\varphi = \mathrm{atan}(\sigma''/\sigma')$). The existence of a phase lag between the current and the voltage is coming from the fact that according to nonequilibrium thermodynamics, the current density depends not only on the electrical field but also on the gradient of the chemical potential of ionic species [*Leroy et al.*, 2008; *Revil and Florsch*, 2010]. When the phase is small (<100 mrad), the phase is given by,

$$\varphi \approx \sigma''/\sigma'. \tag{4}$$

[16] The in-phase conductivity represents the ability of the porous material to transmit electrical current (conduction) while the quadrature conductivity describes the ability of the porous material to store reversibly electrical charges (polarization) under the influence of an electrical field or a current density.

[17] In the following, we will not consider explicitly the frequency dependence of the complex conductivity. Instead, we will take the values of the in-phase and quadrature conductivities at 1 Hz, which is (as shown later) an adequate frequency in probing the polarization of the saprolite. In addition, this frequency is typical of the frequencies used in the field to record resistivity and time-domain induced polarization. The Stern layer polarization model developed by *Revil* [2012, 2013] yields,

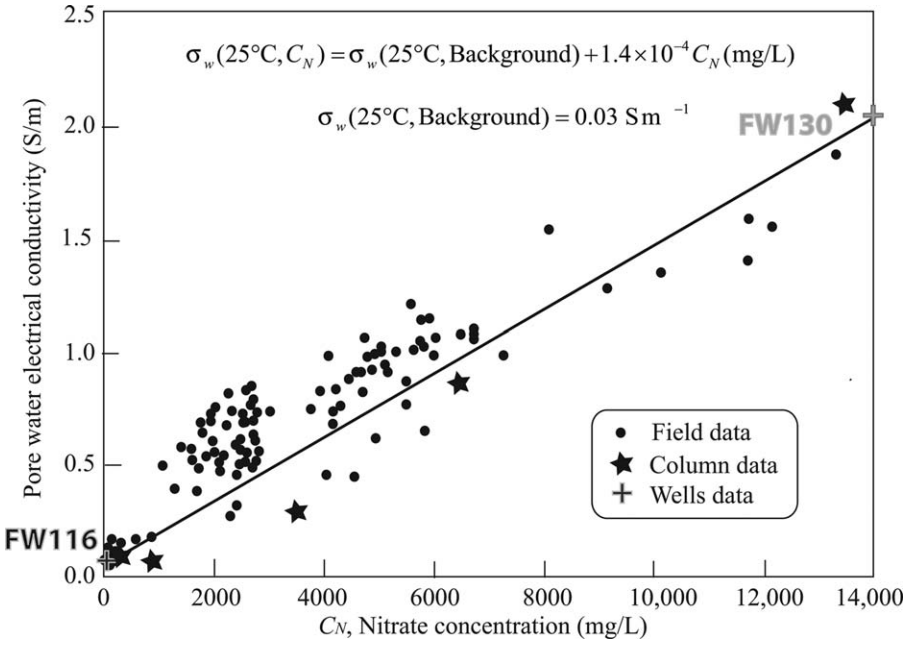

Figure 3. Relationship between the electrical conductivity of the pore water σ_w (in S m^{-1}) and the nitrate concentration C_N (in mg L^{-1}). This relationship respects the value of the conductivity and nitrate concentration in the perched and contaminated aquifers. The measurements have been taken at different dates.

$$\sigma* = \frac{1}{F}\sigma_w + \sigma_S^*. \tag{5}$$

$$\sigma^* = \sigma_w\left(\frac{1}{F} + \mathrm{Du}^*\right). \tag{6}$$

where F denotes the formation factor (dimensionless), σ_w denotes the (real) electrical conductivity of the pore water (in S m^{-1}), σ_S* denotes the complex-valued surface conductivity (components expressed in S m^{-1}), and $\mathrm{Du}^* \equiv \sigma_S^*/\sigma_w$ denotes the complex-valued Dukhin number (unitless, ratio of the complex surface conductivity divided by the pore water conductivity). The formation factor F is related to the connected porosity ϕ by the first Archie's law $F = \phi^{-m}$ with m denoting the cementation exponent [*Archie*, 1942]. According to the Stern layer polarization model, the complex surface conductivity and the complex Dukhin number are defined as,

$$\sigma_S^* = \frac{2}{3}\rho_g \mathrm{CEC}\left[\beta_{(+)}(1-f) - i\beta_{(+)}^S f\right]. \tag{7}$$

$$\mathrm{Du}^* = \frac{2}{3}\left(\frac{\rho_g \mathrm{CEC}}{\sigma_w}\right)\left[\beta_{(+)}(1-f) - i\beta_{(+)}^S f\right]. \tag{8}$$

where f denotes the fraction of counterions in the Stern layer (dimensionless), ρ_g denotes the grain density (typically 2650 kg m^{-3}), $\beta_{(+)}$ denotes the mobility of the counterions in the diffuse layer (equal to the mobility of the same cations in the bulk pore water, $\beta_{(+)}$ (Na^+, 25°C) = 5.2 × 10^{-8} m^2 s^{-1} V^{-1}), and $\beta_{(+)}^S$ denotes the mobility of the counterions in the Stern layer ($\beta_{(+)}^S$(25°C, Na^+) = 1.5 × 10^{-10} m^2 s^{-1} V^{-1}). According to *Revil* [2012], $f \approx 0.90$ for illite and smectite (the salinity dependence of f is discussed in *Revil et al.* [2013c]). The surface conductivity and the Dukhin number are defined as the real part of the complex surface conductivity and the real part of the complex Dukhin number,

$$\sigma_S = \mathrm{Re}\left[\sigma_S^*\right], \tag{9}$$

$$\mathrm{Du} = \mathrm{Re}[\mathrm{Du}^*], \tag{10}$$

respectively. The in-phase conductivity normalized by the pore water conductivity and the phase therefore obey the following relationships,

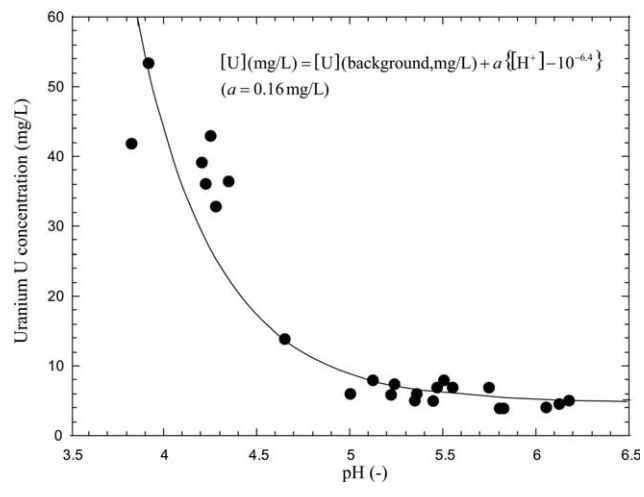

Figure 4. Relationship between the concentration of uranium and the pH of the pore water. This relationship is consistent with the value of the pH and uranium concentration in the perched and contaminated aquifers.

$$\frac{\sigma}{\sigma_w} = \frac{1}{F} + \mathrm{Du}, \tag{11}$$

$$\varphi \approx -\frac{\frac{2}{3}F\beta^S_{(+)}f\rho_g \mathrm{CEC}}{\sigma_w + \frac{2}{3}\beta_{(+)}F(1-f)\rho_g \mathrm{CEC}}, \tag{12}$$

respectively. Following *Revil* [2012, 2013] and *Revil et al.* [2013a], this last equation for the phase can be also approximated by,

$$\varphi \approx -\frac{\beta^S_{(+)}fQ_V}{\sigma_w + \beta_{(+)}(1-f)Q_V}, \tag{13}$$

where the charge density per unit volume is related to the CEC of the material by,

$$Q_V \equiv \rho_g\left(\frac{1-\phi}{\phi}\right)\mathrm{CEC}. \tag{14}$$

[18] In *Revil et al.* [2013c], the salinity dependence of the quadrature conductivity is given by

$$\sigma'' \approx \sigma''_M\left(\frac{C_f K_{\mathrm{Na}}}{1 + C_f K_{\mathrm{Na}}}\right), \tag{15}$$

where,

$$\sigma''_M = -\frac{2}{3}\left(\rho_g \beta^S_{(+)}\Gamma^0_S f\right)S_{sp}. \tag{16}$$

[19] The quantity σ''_M denotes the maximum value of the quadrature conductivity reached at high pH and high salinity values and K_{Na} denotes the apparent sorption constant of Na^+ in the Stern layer of the clay minerals.

3.2. Comparison With Experimental Data

[20] Figure 5 shows that equations (11) and (13) provide a correct representation of the conductivity and phase obtained by *Revil et al.* [2013b]. The formation factor F is in the range of 4–6 (porosity in the range 0.43–0.49), the cementation exponent is in the range of 1.8–2.5, and the surface conductivity is in the range (70–400) $\times$ 10^{-4} S m^{-1}. We will see in section 4 that these values are in contrast with the values obtained on an undisturbed core sample with the contaminated ground water (formation factor of 19.5 at a porosity of 0.37, a cementation exponent of 2.95, and a surface conductivity of 55 $\times$ 10^{-4} S m^{-1}).

[21] In addition to the complex conductivity measurements, we also performed cation exchange capacity (CEC) and specific surface area (using the BET method) measurements on seven saprolitic core samples from the background site of Oak Ridge. The measurements were performed with a barium chloride solution to displace the cations sorbed to the clay mineral surfaces (see protocol in *Sumner and Miller* [1996]). All the seven samples were analyzed in duplicates with relative standard deviation less than 17%. The average measured CEC value of the samples range from 5.0 to 8.6 cmol kg^{-1} or CEC = (4.8–8.3) $\times$ 10^3 C kg^{-1}. The specific surface area is $S_{\mathrm{sp}} = 19{,}000$ m^2 kg^{-1} (measured on same samples from the background site). Taking CEC = 6 $\times$ 10^3 C kg^{-1}, the equivalent total charge per unit surface area is therefore $Q_S = \mathrm{CEC}/S_{\mathrm{sp}} = 0.32$ C m^{-2} (two elementary charges per square nanometer as predicted by *Revil et al.* [1998]). The CEC range reported above together with $\beta^S_{(+)}(25°\mathrm{C}, Na^+) = 1.5 \times 10^{-10}$ m^2 s^{-1} V^{-1}, and $f_M = 0.92$ (high salinity asymptotic value of f) yields $\sigma''_M = -(1.1\text{–}1.9) \times 10^{-3}$S m^{-1} at high salinities, in excellent agreement with the laboratory data shown in Figure 5c (see the high salinity asymptote, $\sigma''_M = -(1.5) \times 10^{-3}$S m^{-1}).

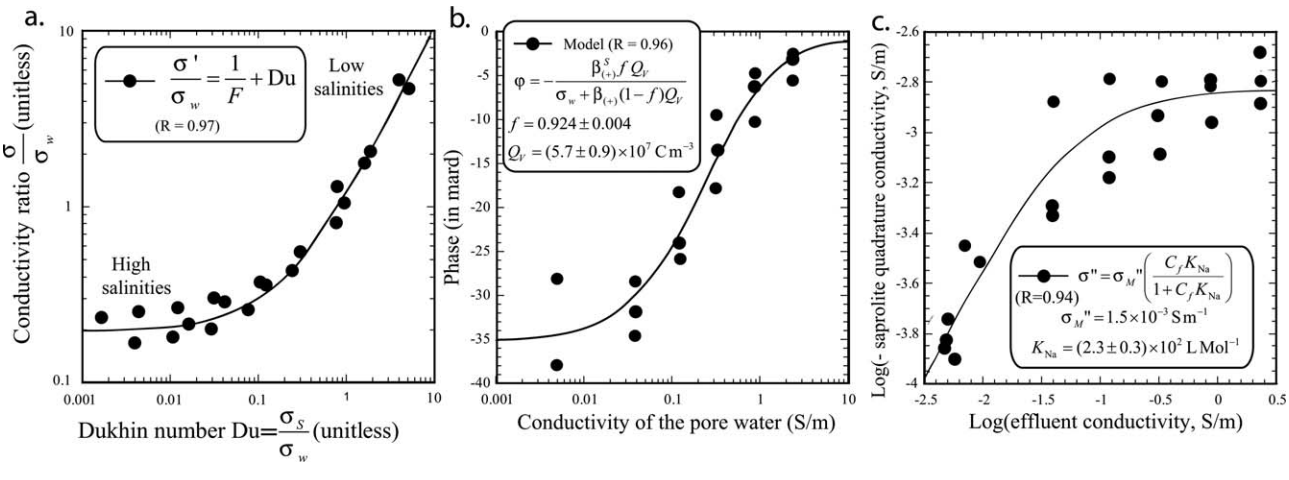

Figure 5. Complex conductivity properties of three core sample of saprolite from Oak Ridge saturated with NaCl solutions. (a) Conductivity ratio (conductivity divided by the pore water conductivity) versus the Dukhin number (ratio of the surface-to-pore water conductivity) for the three-core samples investigated by *Revil et al.* [2013a]. (pH $\sim$ 6). (b) Phase as a function of the conductivity of the pore water for the three-core samples investigated by *Revil et al.* [2013a]. The plain line corresponds to the best fit of the model with a constant partition coefficient f. (c) Dependence of the quadrature conductivity with the conductivity of the effluent (3 saprolite core samples, NaCl, pH $\sim$ 5). The plain line corresponds to the prediction of the model with a Langmuir isotherm for the partition coefficient f.

4. Column Experiment: Material and Methods

4.1. Materials

[22] The saprolite core sample used for the flow-through experiment was collected from Area 3 of the Oak Ridge IFRC (Figure 1c) site at a depth of ~15 m below ground surface in October 2008 (Well FW130, Figure 1d). This material represents the weathered (heavily contaminated) lower part of the saprolite aquifer and characterized by an enhanced permeability with respect to the upper part of the saprolitic aquifer [*McKay et al.*, 2000]. The permeability and hydraulic conductivity values for the column were determined from the differential pressure transducer data and flow rate using Darcy's law. The value of the permeability is $\sim 1.46 \times 10^{-13}$ m^2 (145.8 mD, hydraulic conductivity at 1.39×10^{-6} m s^{-1}, 0.12 m/day). This value is consistent with literature data with a hydraulic conductivity given at 10^{-6} m s^{-1} for the saprolite by *McKay et al.* [2000].

[23] The sample is also coming from an area corresponding to one of the preferential pathways (called CP1 in the nomenclature developed by *Revil et al.* [2013a]) for contaminant migration from the contaminated sediments located below the former S-3 disposal ponds. The porosity of the weathered saprolite ranges from 0.30 to 0.50 [*Jardine et al.*, 1988, 1993; *Wilson et al.*, 1992; *Watson et al.*, 2004] and the porosity of our core sample is 0.37 based on gravimetric measurements performed after the completion of the experiment. The soil sample used in our experiment is actually very typical of what is described as fractured saprolite at the site [*Jardine et al.*, 1988, 1993; *Watson et al.*, 2004]. It is a mixture of fractured rock pieces and fines. Note that only fines were used for the laboratory measurements on the core samples described in section 3 and *Revil et al.* [2013b]. Therefore, the column experiment described below is believed to be more representative of the field conditions than the core samples used by *Revil et al.* [2013b]. The core (~4.3 cm in diameter and 30 cm in length) was caped and stored at 4°C until used for the experiment.

[24] Two types of groundwater were collected for the column experiment. Heavily contaminated ground water was extracted from Well FW130 at a depth of ~15 m, equal to the depth where the core used for the experiment was retrieved. The second ground water sample was collected from the upper portion of the saprolitic aquifer in Well FW116 (located 8 m to the east of FW130). Both waters were collected shortly before the start of the experiment and were kept at 4°C for few days until they were used for the experiment. The first (contaminated) groundwater was used to saturate the core sample while the second water was used to simulate the infiltration of fresh water. The compositions of both ground waters are provided in Table 1.

4.2. Experimental Setup

[25] To minimize disturbances to the sediment pore structure and to preserve the hydraulic properties of the cylindrical core, the sample was used directly for the experiment. Because the sidewall of the core tubing was too thin, a polycarbonate slab was fabricated and glued to the core sleeve for electrode housing. End caps with ports for fluid delivery were installed as well (Figure 6). After the attachment of the polycarbonate slab, four ports were drilled at an interval of 7 cm for setting up the array of Ag/AgCl electrodes. Spectral induced polarization measurements were collected with a National Instruments (NI) dynamic signal analyzer (DSA, NI4461) using electrodes placed along the length of the column (Figure 6). A preamplifier was used to boost the input impedance to 10^9 Ohm to minimize current leakage. Water column calibration and repeatability tests indicate that errors were <0.5 mrads for the phase and 0.5% for resistivity at low frequencies (<1 kHz). Each measurement was composed of a phase lag between the current and the voltage ϕ and a magnitude $|\sigma|$ recorded relative to a precision reference resistor for 40 frequencies spaced at equal logarithmic intervals from 0.1 to 1 kHz.

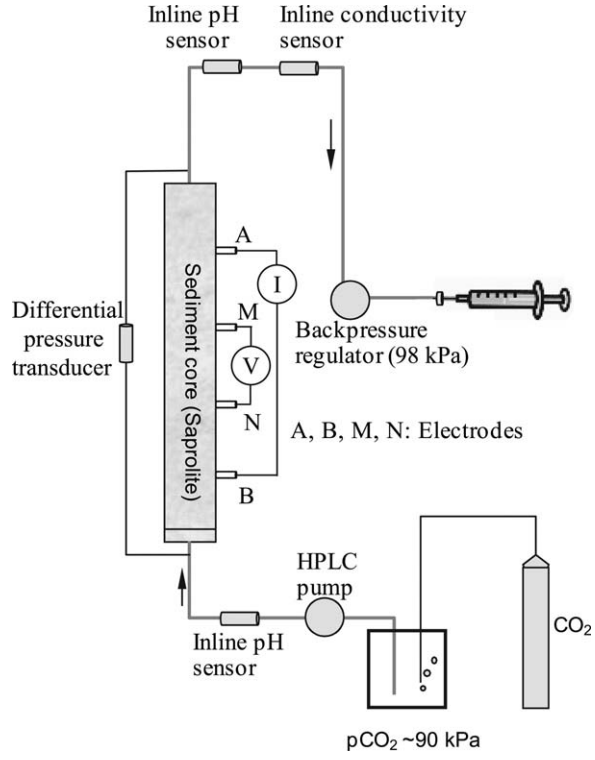

Figure 6. Sketch of the column experiment. The sediment core is made of the Oak Ridge saprolite from the transition zone shown in Figure 2. HPLC denotes the high Performance Liquid Chromatography pump. The sediment core from weathered saprolite zone (FWB130). GW from perched water table (Well FW116) as infiltrating fluid. pCO_2 imposed at ~0.9 atm (90 kPa). Backpressure regulator is used to control pressure/prevent CO_2 outgazing in column. The differential pressure transducer is used to estimate the permeability. Inline pH and conductivity sensor. The flow rate corresponds to 7 days per pore volume (~1.2 mL/h, ~200 mL pore volume). The syringe is used to sample the pore water for geochemical analysis. Complex resistivity measurements: AB current electrodes, MN voltage Ag/AgCl electrodes, V denotes the voltmeter while I denotes the current generator.

[26] In-line pH sensors were used at both ends of the column to monitor pH changes over time and an inline conductivity meter was also installed at the effluent side of the

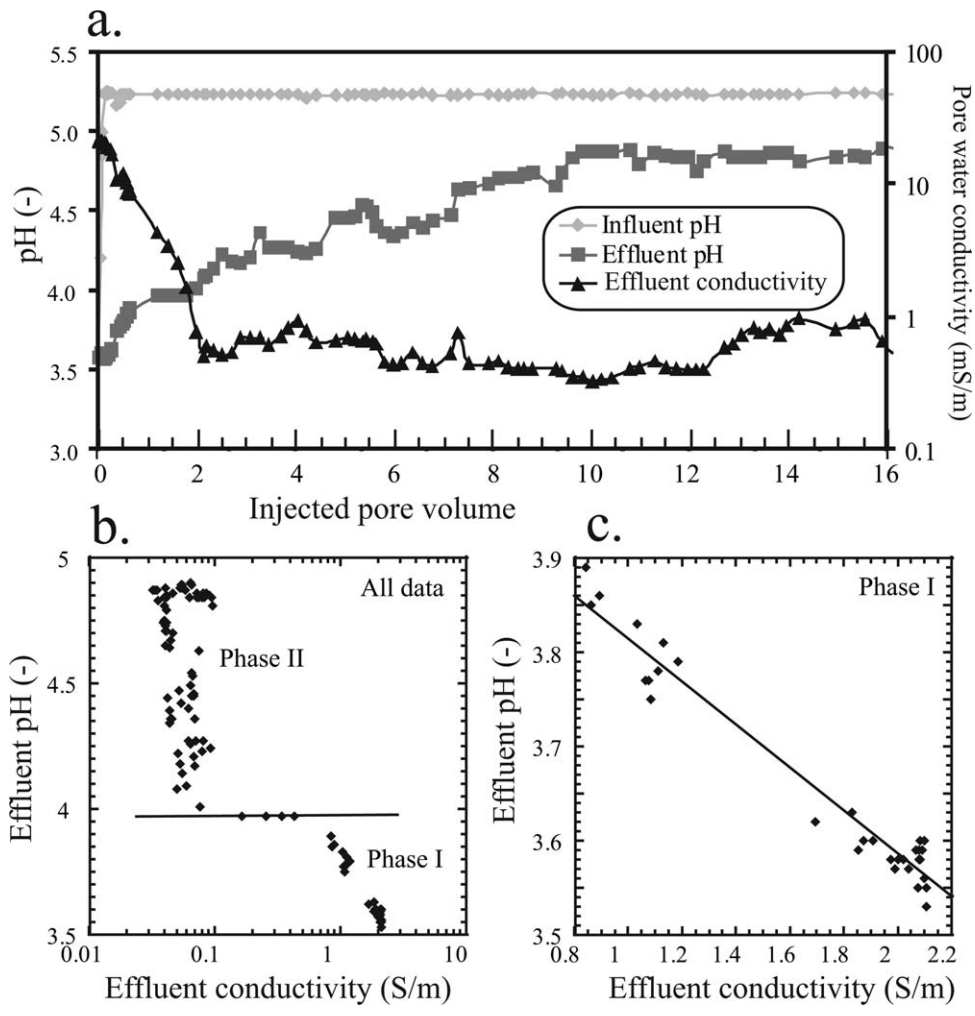

Figure 7. Evolution of the pore fluid properties during the course of the experiment. (a) Changes of pH and conductivity during perched water infiltration. (b) pH versus conductivity of the effluent showing two phases in the flow through experiment: Phase shows a linear dependence between the pH and the pore fluid conductivity while Phase II is characterized by a constant pore water conductivity and a slow change in the pH. (c) pH versus conductivity of the effluent during Phase I.

column to monitor the fluid conductivity (Figure 6). Because of the importance of CO_2 partial pressure (pCO_2) on pH and carbonate species [e.g., *Cai and Reimers*, 1993], in-situ pCO_2 level at ~90 kPa at the weathered saprolite zone (~50 ft below the ground surface) was simulated. The influent fluid reservoir was saturated and bubbled with CO_2 at ~90 kPa and a back pressure regulator was installed at the effluent end to maintain the pCO_2 value within the column. A high-performance liquid chromatography pump was used to deliver the fluids into the column.

[27] After construction, the column was saturated with the groundwater extracted from FW130 to establish the baseline geochemical conditions. After stabilization of the baseline geochemistry (confirmed through repeated pore water chemistry measurements), the relatively fresh water from well FW116 was injected into the column to simulate fresh water infiltration. Spectral induced polarization data were collected automatically using the same system as reported by *Wu et al*. [2011] using a four-electrode approach. Measurements were performed at least once a day, everyday between 10 April 2011 and 18 July 2011. Inline pH and conductivity data were also collected on a daily basis. The injection of the perched water was continued for ~90 days with a total of ~16 pore volumes injected through the sample. The flow rate was about 5.5 days per pore volume (~1.2 mL/h, based on a measured porosity of ~0.366). This flow rate is consistent with a relaxation of the measured resistivity over time with a characteristic time of 19 days. This characteristic time is in turn very comparable to the characteristic time observed in the field for infiltration events as discussed in section 6. Effluent pore water samples were collected with syringes after filtration through a 0.2 μm filter.

[28] The evolution of the pH and conductivity of the effluent are shown in Figure 7a. If the pH of the effluent is plotted as a function of the electrical conductivity of the effluent, there are two phases that can be observed (Figure 7b). Phase I corresponds to a rapid change in both the pH and conductivity of the effluent. In this phase, the pH of the effluent is linearly proportional to the conductivity of the effluent (Figure 7c). In the second phase (Phase II), the pore water conductivity is roughly constant while the pH of

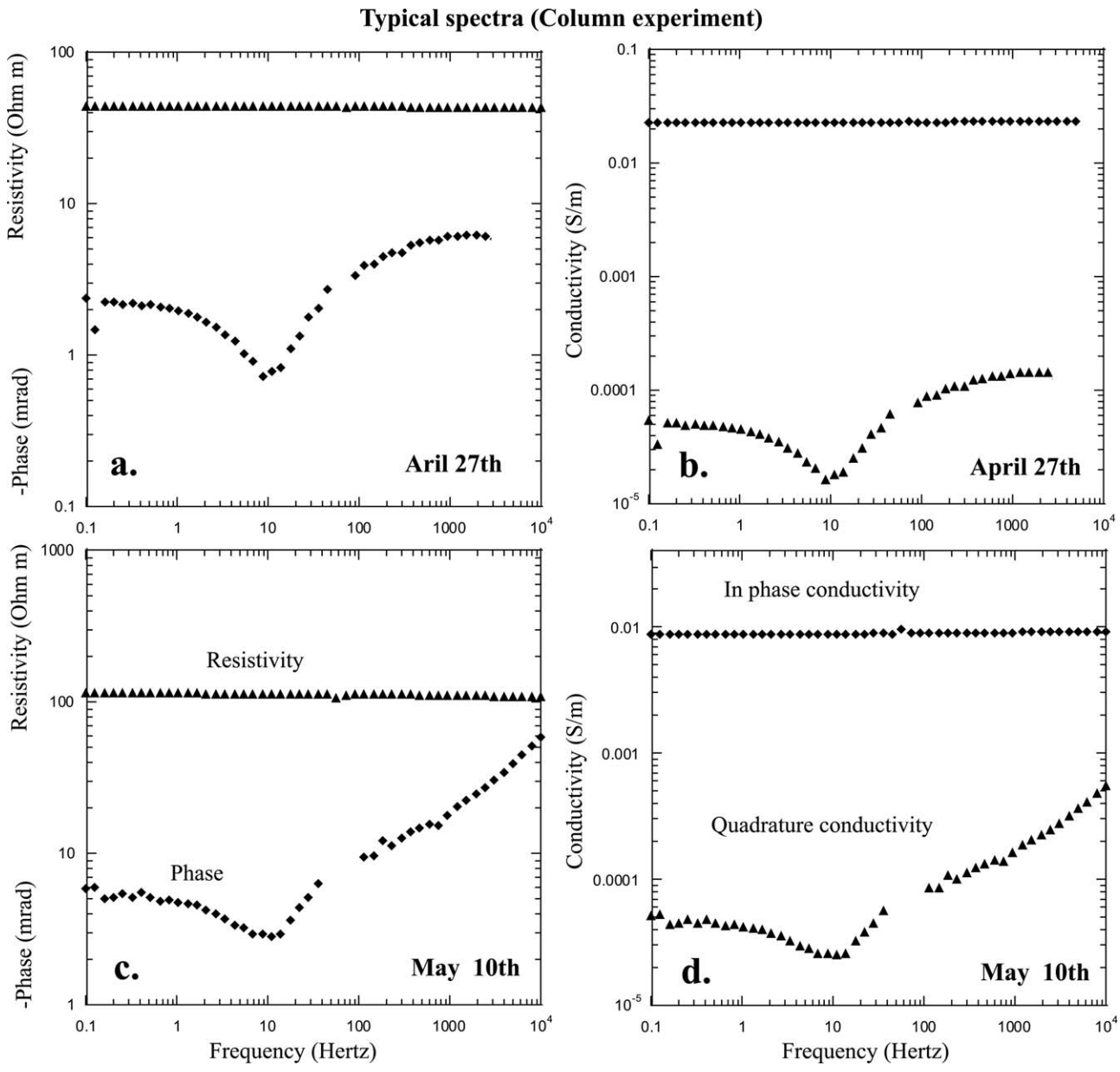

Figure 8. Typical conductivity spectra. The flow through experiment started 10 April. (a, b) Complex conductivity on 27 April (17th day). (c, d) 10 May (30th day). Note the increase of the resistivity from about 40 Ohm m to over 100 Ohm m and the increase of the magnitude of the phase from about −2.3 mrad at low frequencies to about −6 mrad.

the effluent still changes over time. We will see below that the existence of these two phases is useful to analyze the effect of the pore water conductivity and pH upon the quadrature conductivity of the saprolite during the flow-through experiment. We believe that Phases I and II exist also in field conditions for which the system is not in thermodynamic equilibrium or even in steady state conditions as explained below.

4.3. Complex Conductivity Data

[29] Typical complex conductivity spectra taken during the course of the experiment are shown in Figure 8. The resistivity and in-phase conductivity do not depend strongly on the frequency. The phase and the quadrature conductivity show a plateau at low frequencies, then a decrease of their magnitude (∼10 Hz), and finally an increase of their magnitude above 10 Hz. This behavior is quite typical of low-frequency polarization with the low frequency (<10 Hz) behavior being associated with electrical double-layer polarization while the high-frequency behavior is dominated by the Maxwell–Wagner polarization [*Revil*, 2013] shown in the high-frequency part (>10 Hz) in Figure 8. We will report below the data at 1 Hz, which provides a good estimate of the low-frequency polarization.

[30] Figure 9a shows the resistivity and the phase (at 1 Hz) during the course of the experiment. Figure 9b shows the evolution of the in-phase and quadrature conductivities. From Figures 7 and 9b, the in-phase conductivity seems

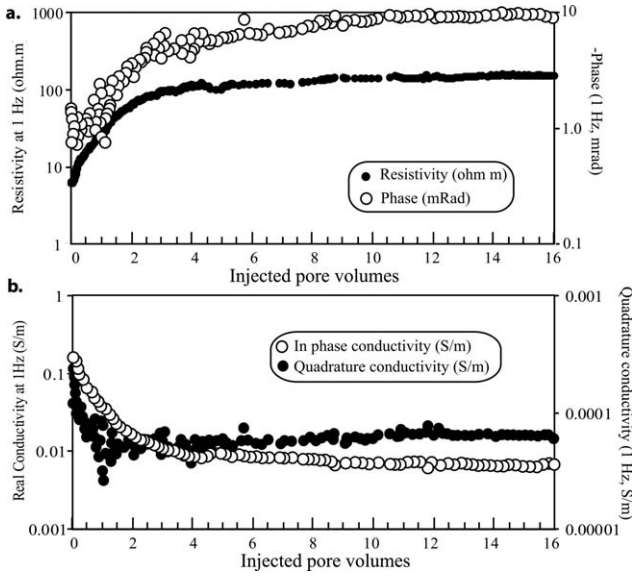

Figure 9. Complex conductivity during the flow-through experiment. (a) Changes of resistivity and phase at 1 Hz during fresh water infiltration sampled from the perched aquifer. (b) Real and imaginary conductivity at 1 Hz during fresh water infiltration sampled from the perched aquifer.

mainly controlled by the pore water conductivity while the quadrature conductivity seems controlled by both the pore water conductivity and the pH. This is quite logical as the pH range investigated, the activity of the protons is too low to impact the pore water conductivity, hence the conductivity of the core sample. In contrast, the quadrature conductivity is sensitive to the complexation of the pore water-mineral interface, which is pH dependent [*Revil*, 2012].

4.4. Geochemical Data Acquisition

[31] During the experiment, effluent samples were collected on regular basis with syringes attached to the outlet of the backpressure regulator (Figure 6). A 0.2-μm filter (to avoid colloidal particles) was used for filtration during sample collection. One milliliter of each sample was acidified with hydrochloric acid for cation analysis using Inductively Coupled Plasma-Mass Spectrometry (ICP-MS). Another milliliter was preserved for major anion analysis using ion chromatography.

5. Column Experiment: Interpretation

5.1. Geochemistry

[32] The evolution of the effluent pH and conductivity is shown in Figure 7a. If the effluent pH is plotted as a function of the effluent conductivity, there are two phases that can be observed (Figure 7b). Phase I corresponds to a rapid change in both the pH and conductivity of the effluent. This change is done to mimic the field conditions that occurred outside thermodynamic equilibrium. In this phase, the pH of the effluent is linearly proportional to the conductivity of the effluent (Figure 7c). In the second phase (Phase II), the pore water conductivity is roughly constant while the pH of the effluent still changes over time. We will see that the existence of these two temporal phases is useful to analyze the effect of the pore water conductivity and pH upon the quadrature conductivity of the saprolite during the flow-through experiment.

[33] The concentration of the major cations and anions are shown in Figures 10 and 11, respectively. The concentration of the effluent for species i is given by,

$$C_i(L,t) = \left(C_i^{\infty} - C_i^0\right)\tilde{C}_i(L,t) + C_i^0, \tag{17}$$

where C_i^0 and C_i^{∞} denote the initial and final concentrations of i, respectively, and the normalized concentration of the effluent $\tilde{C}_i(L,t)$ is obtained by solving the 1D dispersion advection equation [*Shackelford*, 1991],

$$\tilde{C}_i(L,t) = \frac{1}{2}\left\{\mathrm{erfc}\left(\frac{R_d - T}{2\sqrt{\frac{R_d T}{P_L}}}\right) + \exp(P_L)\mathrm{erfc}\left(\frac{R_d + T}{2\sqrt{\frac{R_d T}{P_L}}}\right)\right\}, \tag{18}$$

$$T = \frac{vt}{L}, P_L = vL\overline{D}, \tag{19}$$

$$\overline{D} = D + \alpha v. \tag{20}$$

where v denotes the average pore water velocity (m s^{-1}), t is time (in s), T denotes the number of pore volumes of flow (unitless), P_L the column Peclet number (unitless), L the length of the column (0.3 m), $\overline{D}$ combines the diffusion coefficient (in m^2 s^{-1}), D, and the dispersion coefficient αv (in m^2 s^{-1}) where α denotes the longitudinal dispersivity (in m), and R_d denotes the retardation factor for nonconservative species. When the transport is dominated by advection and dispersion, the Peclet number is $= P_L = L/\alpha$. The function erfc(x) denotes the complementary error function of argument x defined by erfc(x) = 1−erf(x) where erf(x), the error function, is defined by,

$$\mathrm{erf}\,(x) = \frac{2}{\sqrt{\pi}}\int_0^x \exp\left(-\xi^2\right)d\xi. \tag{21}$$

[34] For nonreactive solutes, $R_d = 1$, and therefore, we have,

$$\tilde{C}_i(L,t) = \frac{1}{2}\left\{\mathrm{erfc}\left(\frac{1 - T}{2\sqrt{\frac{T}{P_L}}}\right) + \exp(P_L)\mathrm{erfc}\left(\frac{1 + T}{2\sqrt{\frac{T}{P_L}}}\right)\right\}. \tag{22}$$

[35] Equations (18) or (22) are used to fit the column data for some of the major cations and nitrate (Figure 10). The experimental data agree with a Peclet number $P_L = 3.5 \pm 0.5$. The values of the retardation coefficient are determined for each cation and reported in Table 3. Assuming molecular diffusion can be neglected (it is much smaller than dispersion in the present experiment), the longitudinal dispersivity is given by $\alpha = 0.086$ m.

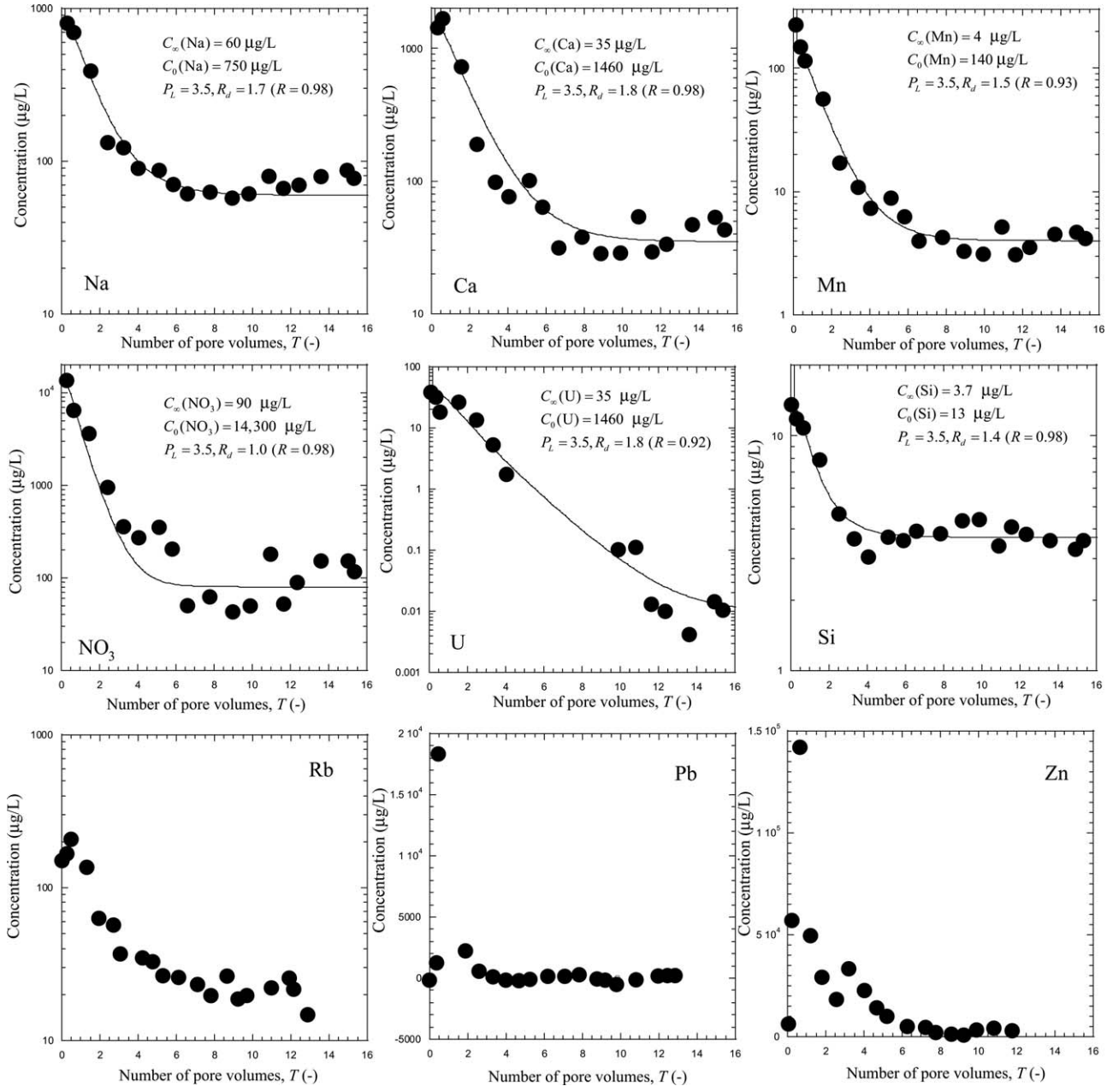

Figure 10. Breakthrough curves of some of the major cations and nitrate. The curves represent the model discussed in the main text and used to estimate the Peclet number and the retardation coefficient. The breakthrough curves for Rb, Pb, and Zn show a peak, typically at one pore volume, corresponding to surface desorption and diffusive transfer from micropores into the fracture porosity.

This value is in agreement with the low range of values reported by *Gwo et al*. [1998] (α in the range 0.08–0.27 m from modeled tracer field experiments at Oak Ridge).

5.2. Conceptual Flow Model

[36] The breakthrough of various species from the geochemical data supports the conceptual flow model established for the weathered saprolite at the Oak Ridge IFRC site: A mixed advective flow through macro- and meso-pores with diffusive transport through low-permeability micropores in soil matrix [*Jardine et al*., 1988, 1993]. The different flow regions are interconnected with flow through fractures. Although the fractures contribute to only 5–10% of the total porosity, it could contain greater than 95% of the pore water flux [*Watson et al*., 2004] due to its high permeability.

[37] Geochemical data (Figures 10 and 11) show rapid decrease of major ion species, e.g., Na^+, Ca^{2+}, and SO_4^{2-}, during the injection of the first pore volume of low ionic strength perched water, indicating the existence of fast flow

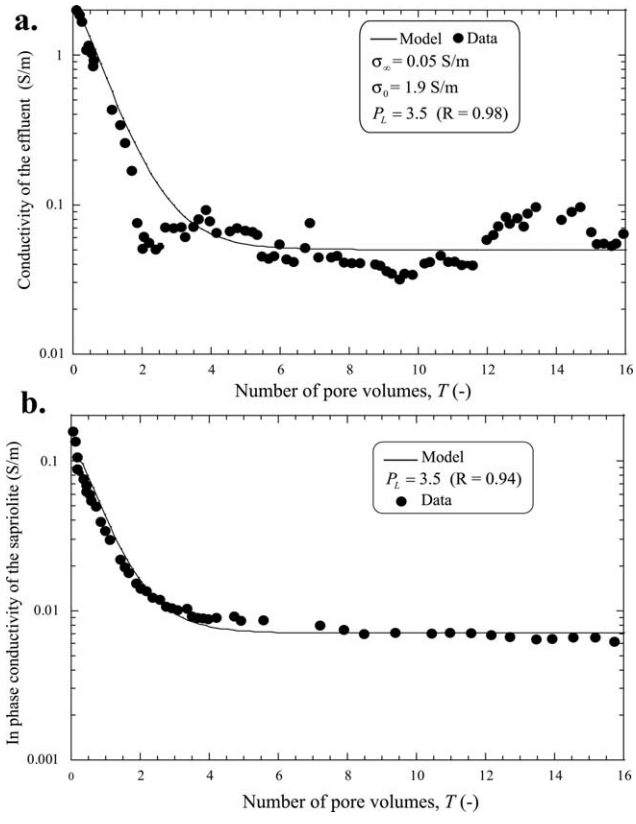

Figure 11. Conductivity versus time for the column experiment. (a) Conductivity of the effluent versus the number of pore volumes *T*. The data are consistent with a Peclet number of 3.5 and a retardation coefficient of 1.0. (b) Conductivity of the saprolite versus the number of pore volumes *T*. The data are consistent with a Peclet number of 3.5 and a retardation coefficient of 1.0, a formation factor of 19.5, and a surface conductivity of 5×10^{-3} S m^{-1}.

paths through the soil column. These fast flow paths interconnect the multiporosity regions that promoted mixing and diffusion transport with the fast flow paths. The combination of advection and dispersion is responsible for the quick breakthrough of major ion species during the injection of the first two pore volume of the perched groundwater. The observed peaks for a few species, e.g., K, Fe, Pb, and Rb (Figure 10), occurred around one pore volume with prolonged tails, which are indications of surface desorption and diffusive transfer from micropores into the fracture porosity.

5.3. In-Phase Conductivity

[38] The evolution of the conductivity of the effluent over time can be described by,

Table 3. Retardation Coefficients R_d for the Cations

Cation	Value
Na	1.7 ± 0.1
Ca	1.8 ± 0.2
U	1.8 ± 0.3
Mn	1.5 ± 0.3
Si	1.4 ± 0.2

Table 4. Petrophysical Properties of the Saprolite From the Transition Zone Between the Saprolitic Aquifer and the Shale Bedrock in the Heavily Contaminated Portion of the Aquifer

Property	Parameter	Value
Porosity	ϕ	0.37 ± 0.01
Permeability	k	1.5×10^{-13} m^2
Hydraulic conductivity	K	1.4×10^{-6} m s^{-1}
Surface area	S_{sp}	19,000 m^2 kg^{-1}
Cation exchange capacity	CEC	5000 C kg^{-1}
Formation factor	F	19.5
Cementation exponent	m	2.95
Longitudinal dispersivity	α	0.086 m

$$\sigma_w(L,t) = \frac{\sigma_w^\infty - \sigma_w^0}{2}\left\{\mathrm{erfc}\left(\frac{R_d - T}{2\sqrt{\frac{R_d T}{P_L}}}\right) + \exp(P_L)\mathrm{erfc}\left(\frac{R_d + T}{2\sqrt{\frac{R_d T}{P_L}}}\right)\right\} + \sigma_w^0. \tag{23}$$

[39] The evolution of the conductivity of the material is therefore given by,

$$\sigma' = \left(\frac{\sigma_w^\infty - \sigma_w^0}{2F}\right)\left\{\mathrm{erfc}\left(\frac{R_d - T}{2\sqrt{\frac{R_d T}{P_L}}}\right) + \exp(P_L)\mathrm{erfc}\left(\frac{R_d + T}{2\sqrt{\frac{R_d T}{P_L}}}\right)\right\} + \frac{\sigma_w^0}{F} + \sigma_S. \tag{24}$$

[40] The in-phase conductivity data are analyzed in Figure 12. In Figure 12a, we show the evolution of the in-phase conductivity and effluent water conductivity. The relationship between the material conductivity and the pore water conductivity is used to determine the formation factor, $F = 19.5$ (reported in Table 4). As discussed by *Revil et al.* [1998], the inverse of the formation factor is exactly the effective porosity of the porous material (therefore 0.05). This effective porosity is therefore significantly lower than the total connected porosity ($\phi = 0.37$). This result is in agreement with the modeling of tracer tests at both laboratory and field scales [see *Jardine et al.*, 1988]. The formation factor and the porosity can be used to determine the cementation exponent using $m = -\ln F/\ln\phi$. We obtain $m = 2.95$ (Table 4), a value higher than the one reported for the fine fraction ($m = 2.2 \pm 0.3$) for the core samples discussed in section 3.

[41] The surface conductivity determined in in Figures 12b and 12c is is 55×10^{-4} S m^{-1}. This value is smaller than for the core samples used from the background site with only the fine portion and with a simple supporting electrolyte (NaCl). This result is logical with respect to the sorption of ionic species in the Stern layer that are less mobile than sodium as discussed by *Vaudelet et al.* [2011a, 2011b]. This shows that a careful consideration of the pore water chemistry is needed if we want to account for the impact of surface conductivity in interpreting electrical resistivity tomograms, a point that has been unfortunately neglected in many studies in hydrogeophysics.

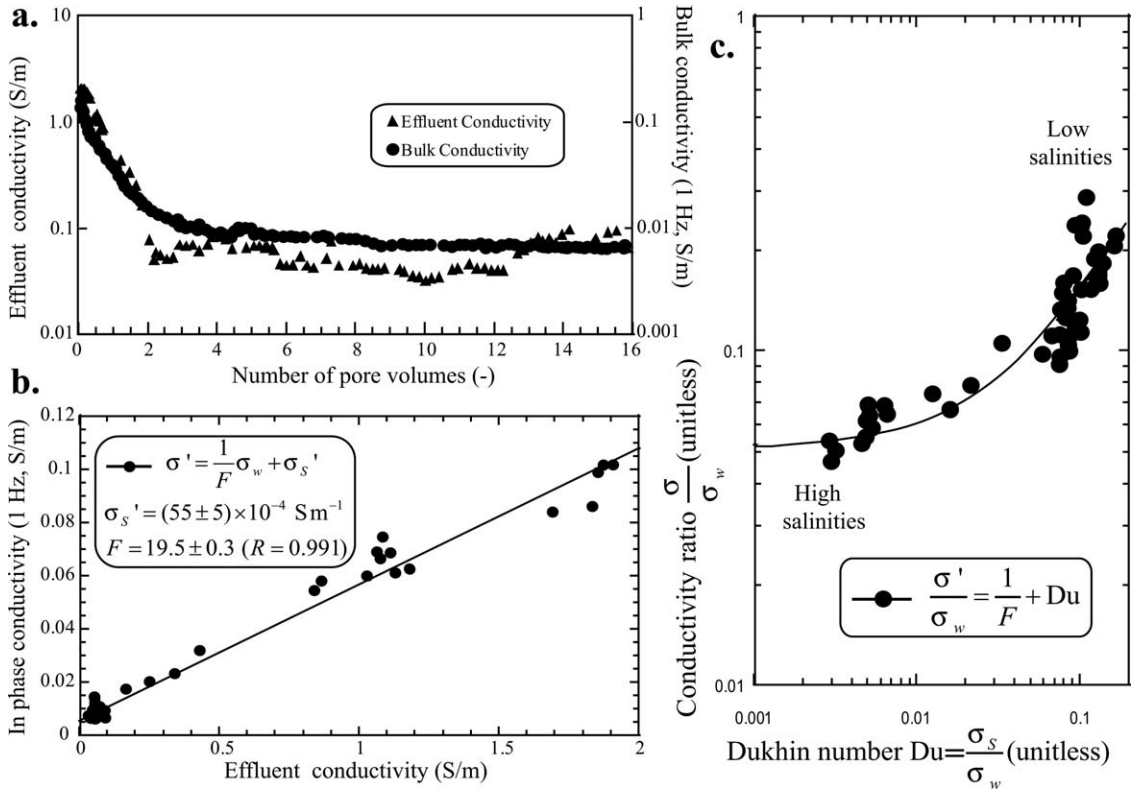

Figure 12. Changes of effluent and bulk conductivity during the experiment. (a) Bulk and in-phase conductivity as a function of the number of pore volume of ground water from the perched aquifer flowing through the saprolite. (b) In-phase conductivity versus the effluent conductivity. The data are used to determine the surface conductivity and the formation factor at 1 Hz. (c) Conductivity data plotted as a function of the Dukhin number. The data are showing that at the end of the experiment, the conductivity is dominated by the surface conductivity.

5.4. Quadrature Conductivity

[42] Figure 13 shows the influence of the pH upon the quadrature conductivity (pore water conductivity $\sim$ 0.07 S m^{-1} at 25°C) in Phase II of the experiment (once the pore water conductivity has stabilized). We clearly see an influence of the quadrature conductivity by the pH of the pore water solution according to,

$$\sigma''(\mathrm{pH}) = -2 \times 10^{-5}(\mathrm{pH} - 1), \tag{25}$$

at a constant pore water conductivity. This indicates the effect of the pH on surface electrochemistry as indicated in *Revil* [2012]. As the quadrature conductivity is controlled by the surface electrochemistry of the Stern layer, this shows the impact of the pH on the sorption of the counterions in the Stern layer (see discussion in *Revil et al.* [2013c]).

6. Application to Field Data

[43] We apply our model to time-lapse resistivity data collected downstream, south of the former S-3 disposal pond during the period 11 November 2008, to 31 January 2009 (see position Figure 14a and *Kowalsky et al.* [2011] and *Gasperikova et al.* [2012], for further details). The direction of the two contaminant plumes CP1 and CP2 (intersecting the resistivity profile) is south west because of the strong anisotropy of the saprolite and the topography of the aquifer–substratum interface while the head gradient is mostly from north to south. Fall 2008 was characterized by strong rain events (Figure 14b). As the result, the ditch surrounding the S-3 pond was partially filled with water in its southern portion and meteoritic water infiltrated the perched aquifer (see Figure 2). In this section, we analyze the time-lapse resistivity data collected during this period using a recently developed method, the active time constrained (ATC) approach [see *Karaoulis et al.*, 2011]. This time-lapse inversion is used to see how the infiltration event of fresh water was recorded in the resistivity time series and how the model described in section 3 and validated in section 4 above can be used to interpret these data.

6.1. Geophysical Data Set

[44] A total of 15 snapshots of apparent resistivity data were obtained downstream the former S-3 Ponds on a portion of Profile P1 (see position Figure 14). Each resistivity data corresponds to 2,568 measurements using the dipole-dipole, Wenner, and Wenner-Schlumberger arrays (38,520 measurements in total). As explained by *Revil et al.*

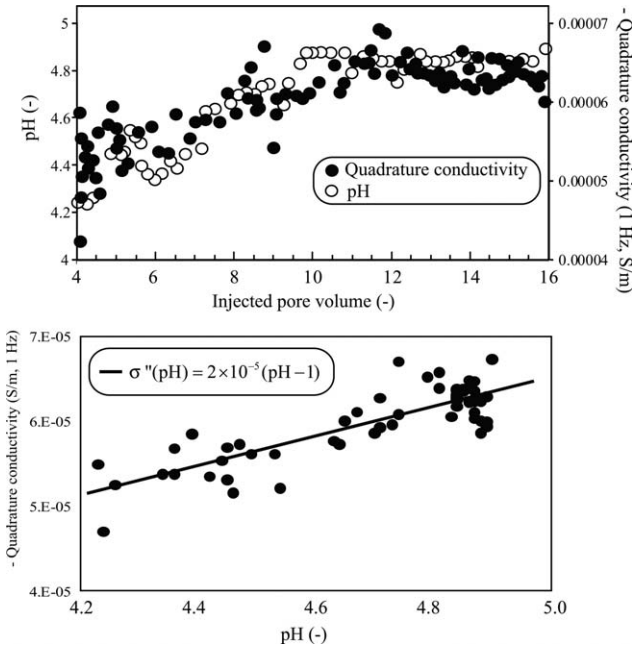

Figure 13. Influence of the pH upon the quadrature conductivity (pore water conductivity ~0.07 S m^{-1} at 25°C) in Phase II. (a) Changes of pH and quadrature conductivity at 1 Hz during the infiltration of the fresh water from the perched aquifer. (b) Correlation between pH and quadrature conductivity at 1 Hz during Phase II of the experiment ($R = 0.84$).

[2013a], each resistivity data set contained both repeated and reciprocal measurements to help identify and remove noisy data. Measurements that differed by more than 3% were removed from the data set prior to the time-lapse inversion. Less than 1% of the repeat and reciprocal measurements had an error > 3%, and less than 10% of the data were removed.

[45] The inversion of the data was performed by using the code developed by *Karaoulis et al*. [2011] using a Gauss-Newton approach. The errors in the data were estimated in the field by repeating the measurements and estimating their standard deviation. These errors were incorporated in a data covariance matrix that was explicitly accounted for in the inversion of the data.

[46] The result of the inversion is shown in Figure 15a. Inversion converged after seven iterations with a data root mean square (RMS) data misfit of 15% (Figure 15b). This RMS error seems high but it is due to random errors in the data likely due to the presence of a grounded generator few tens of meters away from the profile. The inverted tomograms show the position of both the CP1 plume (characterized by low nitrate and high uranium concentrations) and the CP2 plume (characterized by high nitrate and low uranium concentrations).

[47] In Figure 16 and 17, we show the time series for points A and B located in plumes CP1 and CP2, respectively (see Figure 15a). We know that these points belong to the two plumes according to the presence of the wells

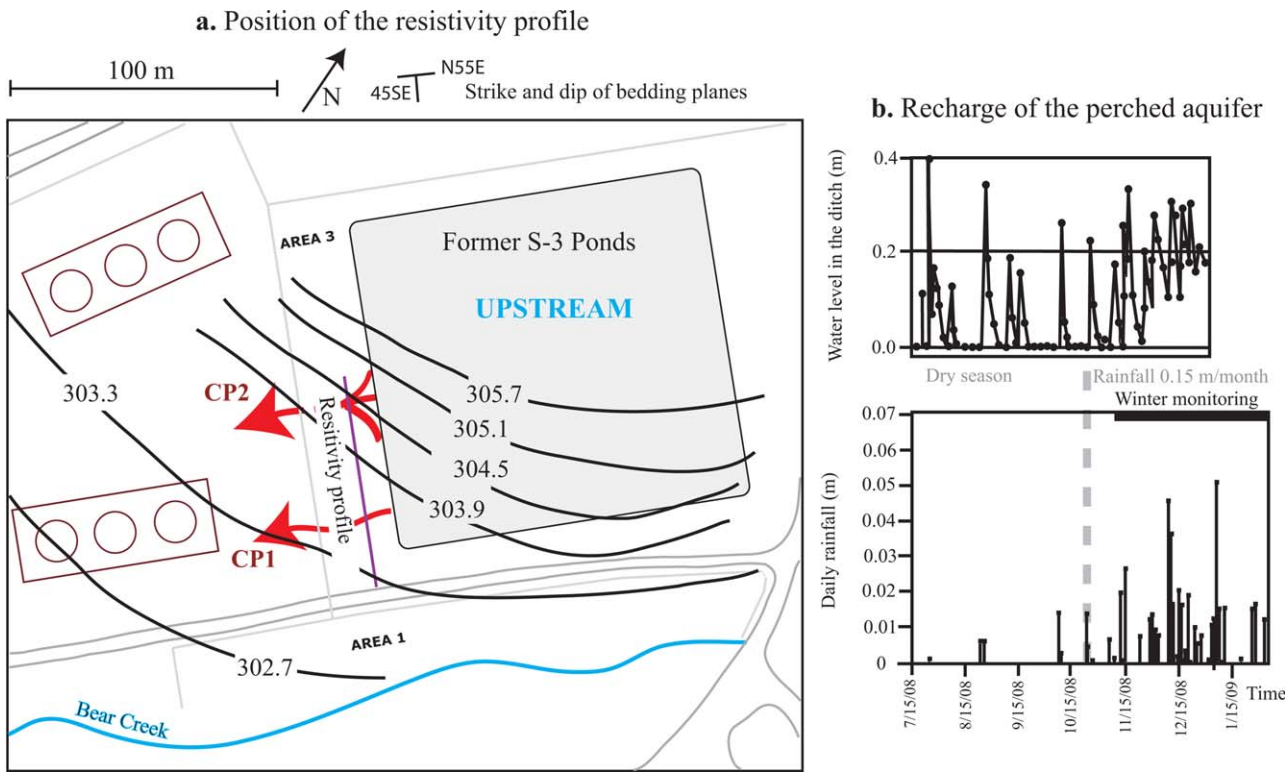

Figure 14. Position of the resistivity profile downstream the former S-3 disposal ponds. (a) Sketch showing the position of the former disposal ponds, the piezometric lever in the saprolitic aquifer (in meters above sea level), and the position of the plumes CP1 and CP2. (b) Water level in the ditch surrounds the former S-3 basins and daily rainfalls showing the recharge of the perched aquifer at the end of 2008. Note that the flow direction is controlled by the fractures along the bedding planes. So the flow is parallel to the bedding planes or strike.

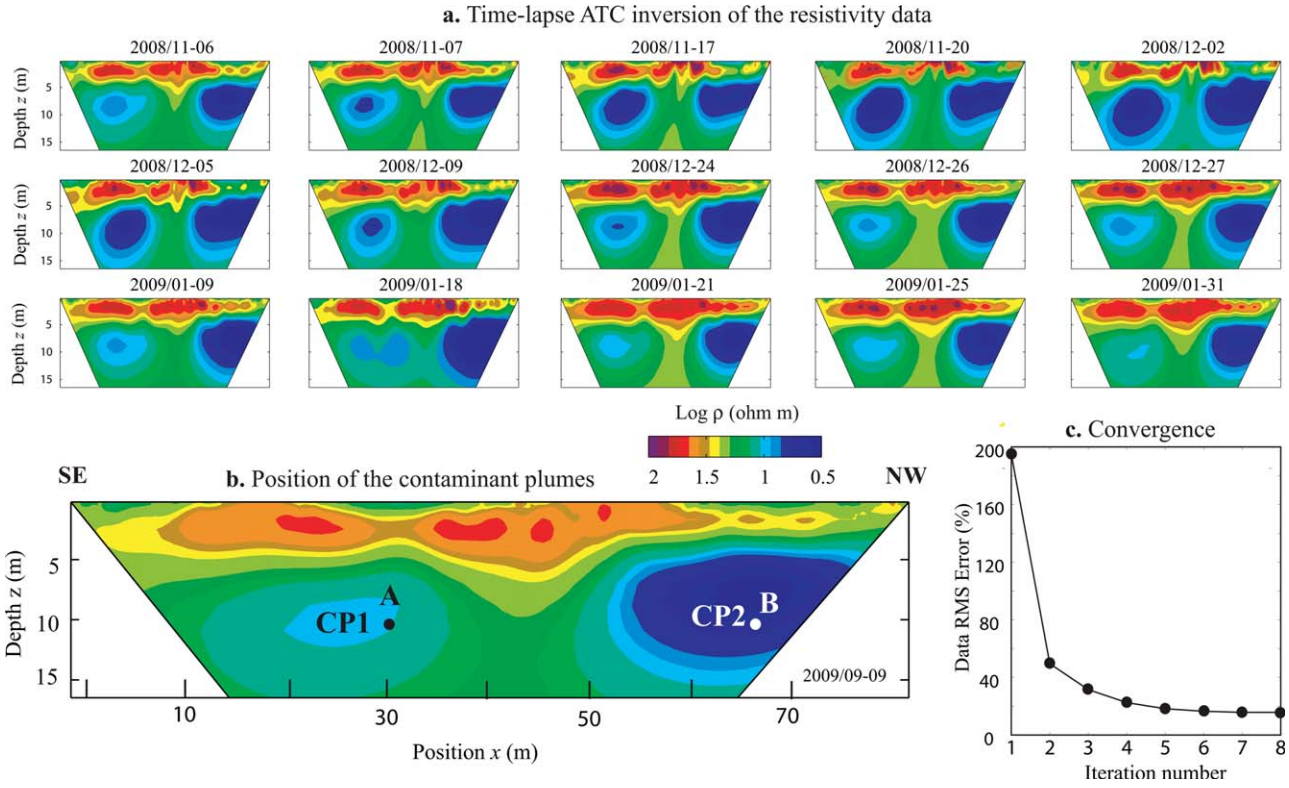

Figure 15. Time-lapse tomography based on the active time constrain (ATC) approach. (a) Results of the time-lapse inversion for a profile located in Area 3 (see Figure 1c). (b) Analysis of a tomogram showing the position of the plumes CP1 and CP2. (c) Data RMS error versus the number of iterations (convergence is reached after seven iterations). The data are in agreement with the variations of the nitrate concentration in the two plumes as discussed by *Revil et al*. [2013a].

nearly. According to the time-lapse resistivity tomograms, the main change in resistivity occurs in CP1, which means that the mixing between the infiltrated water and the original water from the CP1 plume may occur upstream (with respect to the position of the resistivity profile) between the source (the former S-3 disposal ponds) and the position of the resistivity profile. The time-lapse resistivity variations shown in Figure 15a seem to exclude a direct infiltration from the perched aquifer into the deeper portion of the saprolite (the transition zone). Indeed, a gradual infiltration should show a gradual change in the resistivity from the top to the deeper portions of the saprolite over time. Instead we see only changes in the plume CP1 at the depth of the transition zone. This may therefore indicates that the mixing between the fresh water and the contaminated water occurs upstream with respect to the position of the resistivity profile. This possibility will need however to be confirmed.

[48] Before discussing a conceptual model of mixing of the fresh and contaminated waters, we point out that the results displayed by the resistivity tomograms agree with some available and limited in situ observations during this time period. Indeed, Figure 16a shows the dilution of the nitrate plume in Well FW120 during this period. Figure 17 shows that the dilution of the contaminant plume followed an exponential relationship as observed in our column experiment (see Figure 9a).

[49] As mentioned above, our model indicates that the mixing between the fresh and contaminated water occurs in between the position of the resistivity profile and the position of the former S-3 ponds. As shown in Figure 17, this area is the setting of the ditch surrounding the former S-3 basins. Therefore, we think that the ditch plays a major role in the infiltration of the meteoric water and its mixing with the CP1 plume. Indeed, as explained above, the south corner of the ditch surrounding the S-3 basins has the lowest altitudes and therefore is an area where water accumulates preferentially after storms and rainfalls. This may explain why there is some infiltration and mixing for the CP1 plume and not for the CP2 plume. The conceptual model sketched in Figure 18 implies that the fresh water and the contaminated water mixed just below the ditch. The next question to address is how much fresh water mixed with the contaminated water.

6.2. Mixing of End-Members Below the Ditch

[50] We want now to determine how much fresh water mixes with contaminated water in plume CP1. According to our resistivity model (transforming the resistivity into nitrate concentration using a correction for the surface

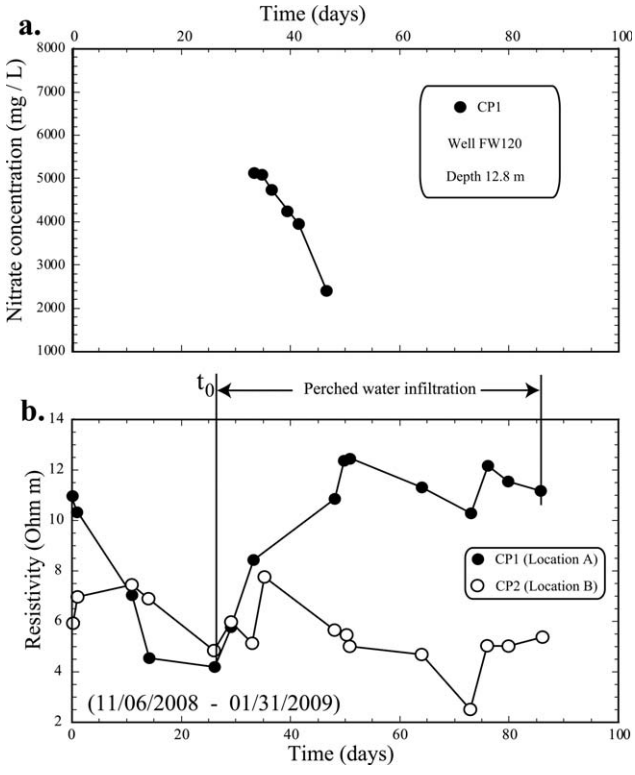

Figure 16. Change of the nitrate concentration and resistivity versus time. (a) Change of nitrate concentration in Well FW120 at a depth of 13.2 m. (b) Field data: Change of resistivity at points A and B (plumes CP1 and CP2) over time. In plume CP1, we see a consistent increase of the resistivity after Day 26 and corresponding therefore to a dilution of the CP1 plume by the infiltration of fresh water from the perched aquifer. Locations A and B are shown in Figure 15.

conductivity), the nitrate concentration of the CP1 plume is 33,000 mg L^{-1} in the absence of mixing with the fresh water and 11,500 mg L^{-1} during steady-state infiltration of the fresh water. This concentration was obtained using the

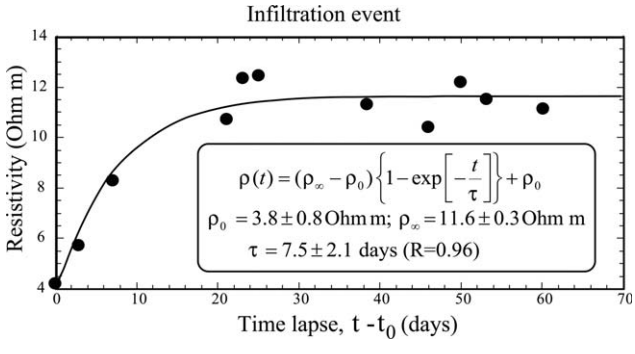

Figure 17. Field data: fit of an exponential relationship to the in situ resistivity data after Day 26. The relaxation time associated with the resistivity change is 7.5 days. This can be compared with a relaxation time of 19.4 days for the laboratory experiment, indicating that the timing of the laboratory column experiment is on the same magnitude as field changes.

following steps: (1) transforming the resistivity into conductivity, (2) determining the conductivity of the pore water using the value of the formation factor in Table 4 and correcting for surface conductivity, and (3) using equation (1) to transform the pore water conductivity into a nitrate concentration. The concentration of nitrate in the fresh aquifer is 0 mg L^{-1}. We can therefore compute how much water from the perched aquifer mixes with the contaminated water from the source of the CP1 plume. During mixing, the nitrate concentration in the mixed pore water $C(\mathrm{NO}_3, \mathrm{mix})$ is given by,

$$C(\mathrm{NO}_3, \mathrm{mix}) = \chi C(\mathrm{NO}_3, \mathrm{CP}\,1), \tag{26}$$

where $C(\mathrm{NO}_3, \mathrm{CP}\,1)$ denotes the concentration in the CP1 plume in the absence of infiltration from the ditch or the perched aquifer (33,000 mg L^{-1}). From equation (26), we have,

$$\chi \approx \frac{C(\mathrm{NO}_3, \mathrm{mix})}{C(\mathrm{NO}_3, \mathrm{CP}\,1)} \approx 0.35. \tag{27}$$

[51] Therefore, during the steady state infiltration into CP1, the pore water may be a mix of one third of the original pore water from the contaminated sediment beneath the former S-3 pond and two thirds of fresh water possibly infiltrating the aquifer from the ditch.

6.3. Proposed Model of Infiltration

[52] With the conceptual model proposed in Figure 18 and the amount of mixing allowed by the infiltration of the fresh water and contaminated water, we can test our model with respect to the resistivity data to see if it is compatible with the properties of the aquifer. Therefore, we use exactly the type of 1-D model used for the column experiment. Initially, contaminated water flows in the CP1 plume. At a certain time, this water is replaced by a mix of one third of the original pore water from the S-3 pond and two thirds of fresh water infiltrating from the ditch. We use equation (24) to fit the time-lapse resistivity data in the plume CP1 (located in the transition zone) using the velocity of the pore water determined from the head gradient in the aquifer (0.02) and the permeability of the aquifer (see value in Table 4). The data are fitted with a Peclet number of 2.3 (Figure 19a) pretty close to the one determined in the flow through experiment (3.5).

[53] In Figure 19b, we predict the variation of the nitrate concentration versus time in plume CP1 showing the transition from 33,000 mg L^{-1} to about 11,000 mg L^{-1}. The addition of complex conductivity data (through frequency-domain or time-domain induced polarization measurements) could also be used to assess the variation of the pH of the pore water versus time during such an infiltration event. Because the meteoritic water ponds at the south corner of the ditch surrounding the former S-3 pond (Figure 14), and not over the entire ditch, infiltration from the ditch affects CP1 and not CP2.

[54] The last question to address is the importance of using the surface conductivity correction in the interpretation of the field data. In the case of plume CP1, the minimum nitrate concentration is about 11,000 mg L^{-1} as discussed above. Using equation (1), this yields a pore

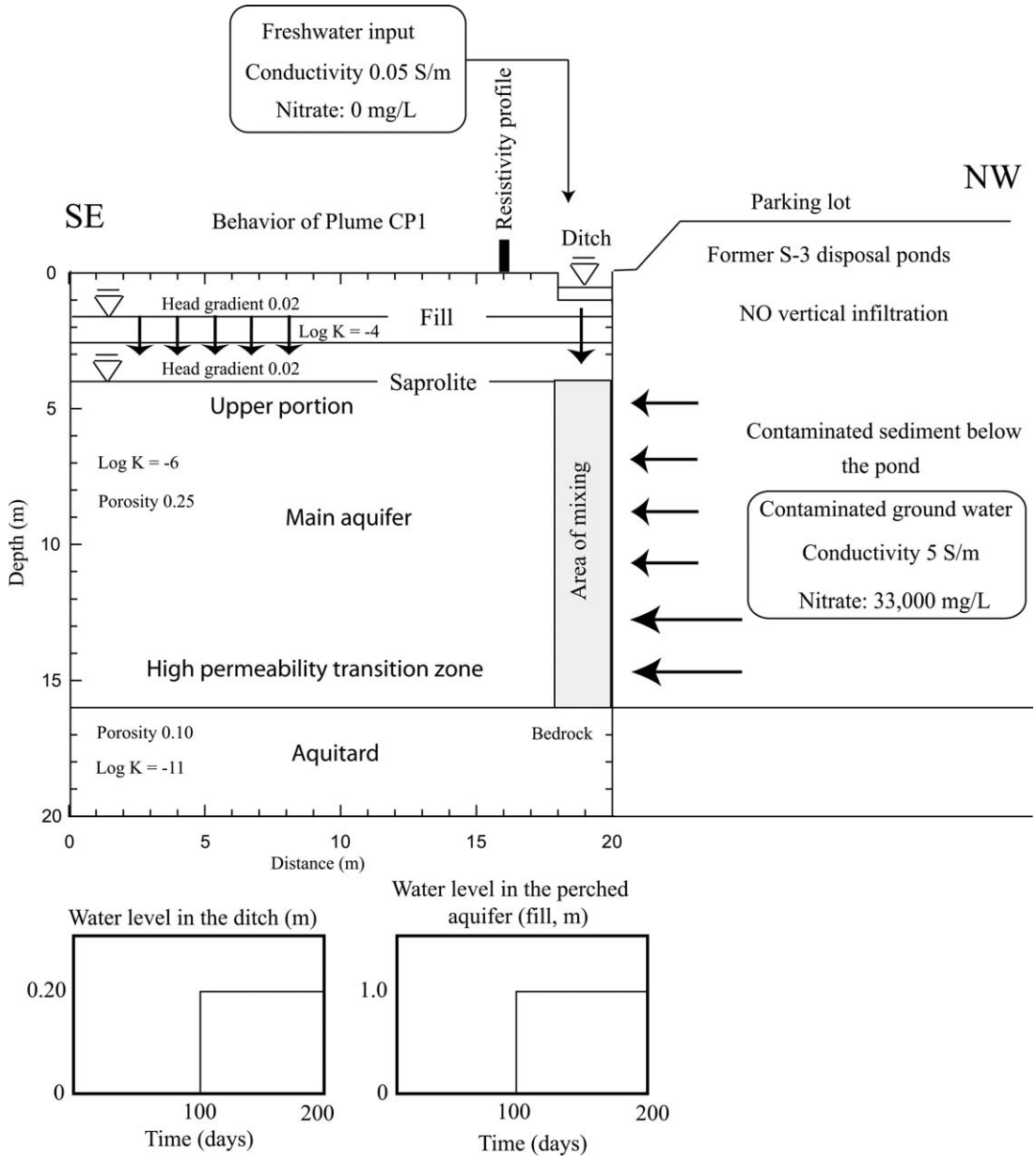

Figure 18. Conceptual model of infiltration in the plume CP1. The ponds are capped with a multilayer cap so there is minimal leaching from above. There is a huge reservoir of contaminants in the saprolite and rock matrix beneath the former disposal ponds and resulting from contamination between 1951 and 1983. The flow of groundwater through the underlying contaminated materials is responsible for the plumes found downstream in the strike direction. Possibly, there is a mixing of this contaminated water with fresh water infiltrating the saprolite from the southern portion of the ditch.

water conductivity of 1.57 S m^{-1}. Using equation (11) with a formation factor of 19.7, the conductivity of the saprolite is 0.081 S m^{-1} without taking into account the surface conductivity and 0.086 in taking into account a surface conductivity of 55×10^{-4} S m^{-1}. Therefore, the difference is about 6%. In this case, the effect of surface conductivity is really a second-order effect in the study of the dilution of the plume associated with the infiltration of the meteoritic water. That said, the background conductivity of the pore water is taken equal to 0.03 S m^{-1} and nearly 20% of this background conductivity is due to surface conductivity. This really shows that surface conductivity needs to be accounted for to understand the background conductivity variations.

7. Conclusions

[55] At the Oak Ridge IFRC site (Tennessee), leaks from the former S-3 disposal ponds have contaminated the saprolite. In 1983, the ponds were drained and filled with fill materials but the contaminated sediments are still releasing contaminant responsible for several contaminant plumes downstream the former ponds. The chemistry of some of these plumes is sometimes disturbed by the infiltration of

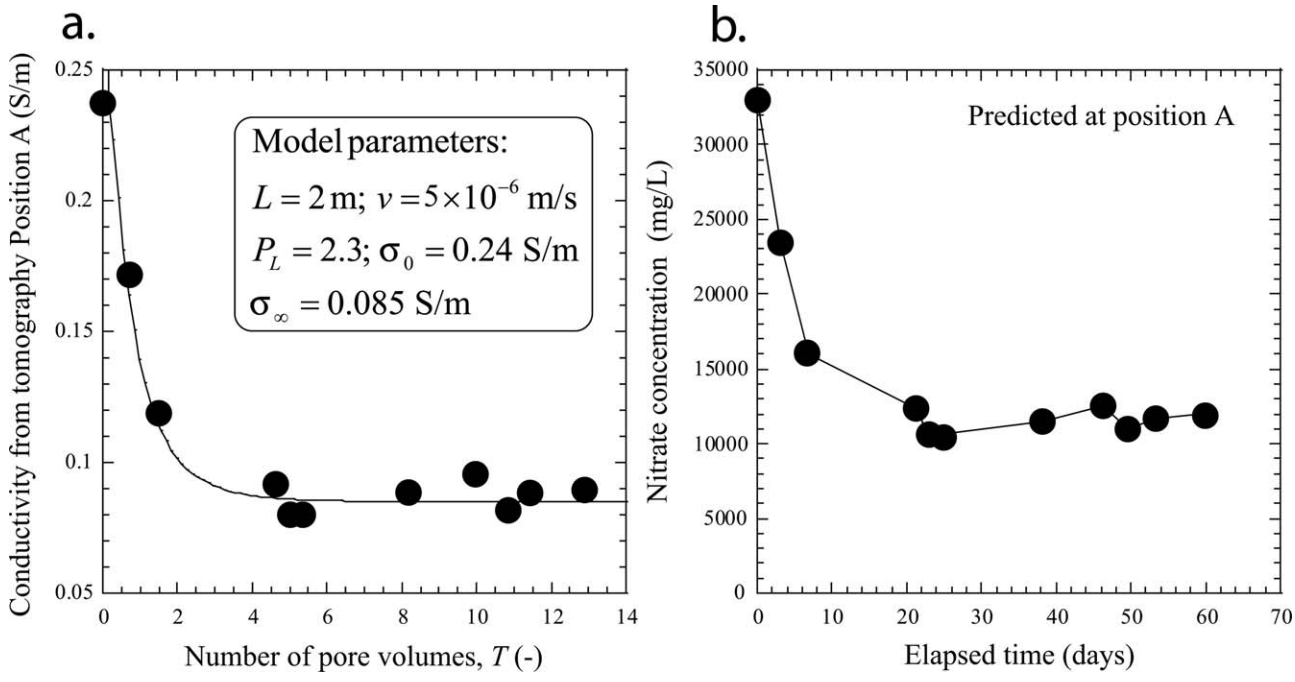

Figure 19. Analysis of the field data. (a) Modeling of the conductivity data in terms of Peclet number, mean pore water velocity at a depth of 10 m (plume CP1, position A, see Figures 14 and 15). The conductivities σ_0 and σ_∞ denote the conductivity of the aquifer at the beginning and end of the infiltration event. The correlation coefficient is $R = 0.94$. Our analysis is performed according to the conceptual model shown in Figure 18. (b) Predicted evolution of the nitrate concentration during the infiltration event.

relatively fresh (meteoritic) water from the upper portion of the saprolitic aquifer. To understand these disturbances (dilution and change in the redox properties), we performed a laboratory experiment. We took a saprolite core sample from the transition zone between the saprolitic aquifer and the shale bedrock in the heavily contaminated portion of the aquifer. This sample was initially saturated with the contaminated ground water from this area. This core sample was then flushed with fresh water collected from the shallow variably saturated perched zone using a time scale comparable to that observed in the field. The following results were obtained:

[56] 1. We found a strong decoupling between the mobile (effective) porosity and the immobile porosity associated with the matrix porosity. The mobile porosity is associated with the presence of cracks in our sample.

[57] 2. Our results suggest that time-lapse induced polarization can be used to analyze the electrical resistivity and the quadrature conductivity in terms of nitrate concentration and pH changes.

[58] 3. We have provided a new set of CEC and specific surface area measurements for the saprolite that can be used in reactive transport modeling codes at this site.

[59] 4. The ATC approach is an efficient tool to filter out the effect of uncorrelated noise in the recorded data set of apparent resistivities. This approach was used to invert a sequence of 15 snapshots used to monitor an infiltration event. Based on this data set, we have determined that during infiltration events the pore water is a mix of one third of the original pore water from the contamination source (S-3 ponds) and two thirds of fresh water at the south portion of the ditch surrounding the S-3 pond.

[60] **Acknowledgments.** We thank the Environment Remediation Science Program (ERSP), U.S. Department of Energy (DOE, award DE-FG02-08ER646559) for funding. The authors appreciate the efforts of Davis Lesmes, the ERSP program manager. We thank Marcella Mueller for her help in getting the Oak Ridge data and samples, Jennifer Earles for the Water levels, Kevin Birdwell for the precipitation data from the ORNL Meteorological Program, and Magnus Skold for his help with the experimental data. We thank the three referees and the Associate Editor for their constructive reviews.

References

Archie, G. E. (1942), The electrical resistivity log as an aid in determining some reservoir characteristics, *Trans. AIME*, *146*, 54–62.

Cai, W. J., and C. E. Reimers (1993), The development of pH and pCO_2 microelectrodes for studying the carbonate chemistry of pore waters near the sediment-water interface, *Limnol. Oceanogr.*, *38*, 1762–1773.

de Lima, O. A. L., and M. M. Sharma (1992), A generalized Maxwell–Wagner theory for membrane polarization in shaly sands, *Geophysics*, *57*, 431–440.

Gasperikova E., S. S. Hubbard, D. B. Watson, G. S. Baker, J. E., Peterson, M. B. Kowalsky, M. Smith, and S. Brooks (2012), Long-term electrical resistivity monitoring of recharge-induced contaminant plume behavior, *Contam. Hydrogeol.*, *142–143*, 33–49.

Grosse, C. (2011), Extension of the classic thin double layer polarization theory of colloidal suspensions to include the stagnant layer conductivity, *J. Phys. Chem. B.*, *115*, 29, 8996–9004.

Gwo, J. P., R. O'Brien, and P. M. Jardine (1998), Mass transfer in structured porous media: embedding mesoscale structure and microscale hydrodynamics in a two-region model, *J. Hydrol.*, *208*, 204–222.

Flores Orozco, A., A. Kemna, C. Oberdörster, L. Zschornack, C. Leven, P. Dietrich, and H. Weiss (2012), Delineation of subsurface hydrocarbon

contamination at a former hydrogenation plant using spectral induced polarization imaging, *J. Contam. Hydrol.*, *136–137*, 131–144.

Jardine, P. M., G. V. Wilson, and R. J. Luxmoore (1988), Modeling the transport of inorganic ions through undisturbed soil columns from two contrasting watersheds, *Soil Sci. Soc. Am. J.*, *52*, 1252–1259.

Jardine, P. M., G. K. Jacobs, and G. V. Wilson (1993), Unsaturated transport processes in undisturbed heterogeneous porous media. I. Inorganic Contaminants, *Soil Sci. Soc. Am. J.*, *57*, 945–953.

Karaoulis M., A. Revil, D. D. Werkema, B. Minsley, W. F. Woodruff and A. Kemna (2011), Time-lapse 3D inversion of complex conductivity data using an active time constrained (ATC) approach, *Geophys. J. Int.*, *187*, 237–251.

Kowalsky, M. B., E. Gasperikova, S. Finsterle, D. Watson, G. Baker, and S. S. Hubbard (2011), Coupled modeling of hydrogeochemical and electrical resistivity data for exploring the impact of recharge on subsurface contamination, *Water Resour. Res.*, *47*, W02509, doi:10.1029/2009WR008947.

Leroy P., A. Revil, A. Kemna, P. Cosenza, and A. Ghorbani (2008), Spectral induced polarization of water-saturated packs of glass beads, *J. Colloid Interf. Sci.*, *321*(1), 103–117.

McKay, L.D., W. E. Sanford, and J. M. Strong (2000), Field scale migration of colloidal tracers in a fractured shale saprolite, *Ground Water*, *38*(1), 139–147.

Revil, A. (2012), Spectral induced polarization of shaly sands: Influence of the electrical double layer, *Water Resour. Res.*, *48*, W02517, doi:10.1029/2011WR011260.

Revil, A. (2013), Effective conductivity and permittivity of unsaturated porous materials in the frequency range 1 mHz–1GHz, *Water Resour. Res.*, *49*, 306–327, doi:10.1029/2012WR012700.

Revil, A., and L. M. Cathles (1999), Permeability of shaly sands, *Water Resour. Res.*, *35*(3), 651–662.

Revil, A. and N. Florsch (2010), Determination of permeability from spectral induced polarization in granular media, *Geophys. J. Int.*, *181*, 1480–1498, doi:10.1111/j.1365-246X.2010.04573.x.

Revil, A., L. M., Cathles, S., Losh, and J. A., Nunn (1998), Electrical conductivity in shaly sands with geophysical applications, *J. Geophys. Res.*, *103*(B10), 23,925–23,936.

Revil, A., M. Skold, M. Karaoulis, M. Schmutz, S. S. Hubbard, T.L. Mehlhorn, and D. B. Watson (2013a), Hydrogeophysical investigations of the former S-3 ponds contaminant plumes, *Geophysics*, 78(4), EN29-EN41, doi: 10.1190/geo2012-0177.1.

Revil, A., M. Skold, S. Hubbard, Y. Wu, D. Watson, and M. Karaoulis (2013b), Petrophysical properties of saprolites from the Oak Ridge Integrated Field Research Challenge site, *Tennessee, Geophysics*, *78*(1), D21–D40.

Revil, A., J. D. Eppehimer, M. Skold, M. Karaoulis, L. Godinez, and M. Prasad (2013c), Low-frequency complex conductivity of sandy and clayey materials, *J. Colloid Interface Sci.*, *398*, 193–209.

Shackelford, C. D. (1991), Laboratory diffusion testing for waste disposal-A review, *J. Contam. Hydrol.*, *7*, 177–217.

Shevenell, L. A., G. K. Moore, and R. B. Dreier (1994), Contaminant spread and flushing in fractured rocks near Oak Ridge, Tennessee, *Groundwater Monit. Remediation*, *14*, 120-129.

Sumner, M. E., and W. P. Miller (1996), Cation Exchange Capacity and Exchange Coefficients, in *Methods of soil analysis Part 3: Chemical Methods*, edited by D. L. Page, pp. 517–550, Soil Sci. Soc. of Am., Madison, Wis.

Vaudelet P., A. Revil, M. Schmutz, M. Franceschi, and P. Bégassat (2011a), Induced polarization signature of the presence of copper in saturated sands, *Water Resour. Res.*, *47*, W02526, doi:10.1029/2010WR009310.

Vaudelet P., A. Revil, M. Schmutz, M. Franceschi, and P. Bégassat (2011b), Changes in induced polarization associated with the sorption of sodium, lead, and zinc on silica sands, *J. Colloid Interface Sci.*, *360*, 739–752.

Watson, D. B., J. E. Kostka, M. W. Fields, and P. M. Jardine (2004), *The Oak Ridge Field Research Center Conceptual Model, NABIR FRC Technical Report: NABIR FRC,* DOE, Oak Ridge, Tenn. [Available at http://public.ornl.gov/orifc/FRC-conceptual-model.pdf.]

Weller A., K. Breede, L. Slater and S. Nordsiek (2011), Effect of changing water salinity on complex conductivity spectra of sandstones, *Geophysics*, *76*(6), F315–F327.

Wilson, G. V., P. M. Jardine, and J. P. Gwo (1992), Modeling the hydraulic properties of a multi-region soil, *Soil Sci. Soc. Am. J.*, *56*, 1731–1737.

Wu, Y., J. B. Ajo-Franklin, N. Spycher, S. S. Hubbard, G. Zhang, K. H. Williams, J. Taylor, Y. Fujita, and R. Smith (2011), Geophysical monitoring and reactive transport modeling of ureolytically-driven calcium carbonate precipitation, *Geochem. Trans.*, *12*(7), doi:10.1186/1467-4866-12-7.